A FEM-BEM coupling strategy for the modeling of magnetoelectric effects in composite structures

A Urdaneta-Calzadilla, N Galopin, Innocent Niyonzima, I Niyonzima, Olivier Chadebec, B Bannwarth, Gérard Meunier

▶ **To cite this version:**

A Urdaneta-Calzadilla, N Galopin, Innocent Niyonzima, I Niyonzima, Olivier Chadebec, et al.. A FEM-BEM coupling strategy for the modeling of magnetoelectric effects in composite structures. Engineering Analysis with Boundary Elements, 2023, 151, pp.41-55. hal-03798171v1

HAL Id: hal-03798171

https://hal.science/hal-03798171v1

Submitted on 5 Oct 2022 (v1), last revised 28 Feb 2023 (v2)

HAL is a multi-disciplinary open access archive for the deposit and dissemination of scientific research documents, whether they are published or not. The documents may come from teaching and research institutions in France or abroad, or from public or private research centers.

L'archive ouverte pluridisciplinaire **HAL**, est destinée au dépôt et à la diffusion de documents scientifiques de niveau recherche, publiés ou non, émanant des établissements d'enseignement et de recherche français ou étrangers, des laboratoires publics ou privés.

A FEM-BEM coupling strategy for the modeling of magnetoelectric effects in composite structures

A. Urdaneta-Calzadilla, N. Galopin, I. Niyonzima, O. Chadebec, B. Bannwarth, G. Meunier

[a] *Univ. Grenoble Alpes, CNRS, Grenoble INP, G2Elab, F-38000 Grenoble, France*

Abstract

This paper deals with the modeling of devices based on magnetoelectric composite materials. These heterogeneous structures are made of ferromagnetic and ferroelectric materials, the mechanical coupling of which allows obtaining magneto-electric effects exceeding by several orders of magnitude the response of single-phase components. A coupling of the Finite Element Method (FEM) and the Boundary Element Method (BEM) is used to model the behavior of magnetic effects, while classical FEM formulations are used for the electrical and mechanical problems. This coupling of numerical methods allows to avoid considering a free space domain around the active domain, and thus to use a single mesh for the magnetic, mechanical and electrical problems. This results in a consequent reduction of the number of unknowns, which is accompanied by shorter computation times compared to a pure FEM approach. The global algebraic system is solved by a block Gauss-Seidel type solver, which allows a good convergence of the multiphysics.

Keywords:
FEM-BEM coupling, electro-magneto-mechanical, magnetoelectric composite, block Gauss-Seidel solver

1. Introduction

Energy conversion in electrical transducers or actuators is based on electromagnetic interactions, which link the electromotive force to temporal variations of the magnetic flux density. However, these phenomena are sometimes difficult to exploit, especially for small devices submitted to very low

frequency fields. The use of active composite structures, in particular, magnetoelectric (ME) composite structure can help address this issue [1].

The ME coupling consists in the existence of an electric polarization induced by a magnetization or, conversely, of a magnetization induced by an electric polarization. Materials with such properties have opened up possibilities of new applications in various fields, such as magnetic field sensors [2], tunable radio-frequency magnetic filters [3], antennas [4], gyrators [5], energy harvesters [6], memory devices based on the principle of electric writing-magnetic reading [7, 8], biology and medicine [9]. This interaction emerges as a material property and does not follow directly from Maxwell's equations. Past research has been conducted in order to obtain single-phase materials that simultaneously exhibit coupled magnetic and electrical ferroic orders, also known as multiferroics. Unfortunately, despite many efforts and with few exceptions [10], the majority of single-phase multiferroic materials are made of complex oxides that exhibit very low coefficients and mainly at low temperatures [11, 12]. It has been shown that ordinary magnetic and electrical susceptibilities provide an upper bound on the coefficient for single-phase magnetoelectric materials [13]. This disadvantage has been successfully overcome by the fabrication of magnetoelectric composites which consist of coupled magneto-mechanical and electro-mechanical phases [14, 15], the resulting heterogeneous materials show large ME coefficients. The aim of such composites is to generate the intended magnetoelectric effect as a deformation-induced product property [16], property that their individual constituents do not have. In the direct ME effect an applied magnetic field causes a deformation of the magneto-mechanical coupled phase which is transmitted to the electro-mechanical coupled phase. As a result, a strain-induced polarization modulation in the electric phase is obtained. While in the inverse effect, an applied electric field causes a deformation of the electro-mechanical phase which is then transmitted to the magneto-mechanical phase (reverse effect). This results in strain-induced magnetization modulation.

The behavior, performance and effective properties of magnetoelectric composites depend on the material composition of each phase, the bonds between the different phases, their morphology and the electrical resistance of the composite. The electro-mechanical coupled phases can be composed of ferroelectric (FE) materials ($BaTiO_3$, $PbTiO_3$, $Pb(Zr,Ti)TiO_3$) or piezoelectric materials (PE) ((1-x)Pb(Mg1/3Nb2/3)$O_{3-x}$$PbTiO_3$ (PMN-PT), PZT),

while the magneto-mechanical coupled phases can be made of ferrimagnetic (FI) ($CoFe_2O_4$, $NiFe_2O_4$) or ferromagnetic (FM) materials (CoFeB, FeGa). These heterostructures can be either multiferroic (and also magnetoelectric), comprising FE/FM materials, or magnetoelectric but not multiferroic, i.e., having only one ferroic order, often with PE/FM materials. Particulate composites formed from a microscale mixture of FE and FI materials show magnetoelectric coefficient values between 1 and 500 mV cm^{-1} Oe^{-1} at low frequencies [17], while larger values are obtained at mechanical resonance [18]. In comparison, laminated composites composed of the same ferroelectric and ferrimagnetic materials show magnetoelectric coefficient values that are an order of magnitude higher. The highest magnetoelectric coupling coefficients (> 5 V Cm^{-1} Oe^{-1}) are obtained by layered heterogeneous structures whose magneto-mechanical phase is composed of either a giant magnetostriction alloy (Terfenol-D: $Tb_{1-x}Dy_xFe_2$) [19] or an amorphous alloy with high magnetic permeability and piezomagnetic coefficients (Metglass: Fe-based alloys) [20]. For the manufacture of laminated composites based on ceramics and alloys, co-sintering and bonding are the most popular methods.

The complex behavior of the magnetoelectric composite materials described above involves not only the definition of appropriate material models, but also the formulation and solution of fully coupled boundary-value problems, especially for the development of technological applications. Several approaches including analytical methods, semi-analytical methods and numerical methods have been applied to the prediction of the overall material properties and to the investigation of the coupling behavior of the magnetoelectric materials.

Analytical approaches based on Green's functions have been proposed for example by Nan et al. [21, 22, 23], Pan [24], Wang and Shen [25]. Elastodynamics methods combining the equation of motion of continuous media with mechanical and electrical boundary conditions have also been proposed, for example by Harshé et al. [26], Avellaneda and Harshé [27], Wu et al. [28], Muchenik and Barbero [29]. In the previous approach, the response of ME materials was studied assuming linear behaviors for the ferroelectric and ferromagnetic phases. These models have shown how the volume fractions of each phase, the connectivity [30], as well as the piezoelectric, piezomagnetic and elastic properties participate in the ME coupling. The nonlinear response and stress dependence of the ME composite are addressed, for example, by

Wang and Zhou [31], Lin et al. [32], Burdin et al. [33], Shi et al. [34] who considered the nonlinear anhysteretic behavior and the effect of stress in the constitutive relationships of the ferromagnetic phase. It results from these approaches a way to improve the ME coefficients and the frequency-multiplying behavior of laminated composites via magnetic bias field and pre-stress. The interfaces between ferroelectric and ferromagnetic phases, which are not perfect and usually corresponds to a layer of epoxy glue, are accounted for by means of an interface coupling factor [35, 31]. Taking these interface effects into consideration allows for better prediction of the coupling behavior of ME composites.

Approaches based on the method of equivalent electrical circuits have also been proposed [36, 37]. They use an extension of Mason's model which allows to establish an equivalent electrical circuit of the ME composites, whose equivalent electrical parameters are established via a coupled equation of motion and the integration of the piezoelectric and magnetostrictive behavior laws. More specifically, these methods can be used to investigate the voltage ME coefficient for different modes in static or dynamic regimes and the electrical resistance load effect on the resonant ME coupling.

To describe and predict the behavior and effective properties of ME composites considering the microstructures and anisotropies of the materials, various micromechanical analyses have been developed. Such analytical or semi-analytical solutions are for example based on the homogenization and self-consistent models [38, 39, 40, 41, 42], Mori-Tanaka mean field theory [43, 44], variational asymptotic approach [45, 46] or Eshelby's equivalent inclusion approach [47, 48].

All the previously described methods allow to study ME composites with trivial geometries such as composites with perfect ellipsoidal inclusions, perfect laminated structures or composites involving simple boundary value problems. Despite being computationally expensive, numerical tools are not restricted to specific topologies. Simulation based on FEM have been conducted for example, by Buchanan [49] and Galopin et al. [50] to study the multilayer and multiphase ME composites response, and by Lee et al. [51], Avakian et al. [52] and Zhang et al. [53] in order to determine the effective properties of linear and non-linear multiphase ME composites. Nevertheless, a classical FE approach can become unsuitable for modeling ME devices with several disadvantages.

One disadvantage is related to the stray magnetic fields from the sources and ME composites. For simple geometries, these stray fields are linked to the geometry and proportional to the magnetization level. They can be accounted for by demagnetizing coefficients. This is no longer possible for more complex geometries or source configurations and the treatment of an open boundary problem is required. Due to the decrease of the field away from the sources, an intuitive approach is to consider a sufficiently large but finite free space domain to respect the conditions of field cancellation at infinity. Methods for treating open boundary problems have been developed including those involving infinite elements [54, 55] but they still require the presence of a free space domain which may lead to a huge mesh.

A second disadvantage of FEM is related to specific applications where the sources of the magnetic fields commonly known as inductors are located far from the active materials. An even larger free space domain containing both the field sources and the ME composite is needed. The free space domain can then be much larger than that associated with active materials. On the other hand, for problems with a huge free space domain compared to the active structure, the FEM leads to problems of accuracy and convergence [56].

These problems can be avoided by coupling FEM with the BEM. This coupling of numerical methods is particularly well adapted to the numerical resolution of open boundary electromagnetic problems. For linear problems involving homogeneous materials embedded in free space, only the boundaries of the material domain needs to be discretized. The FEM-BEM approach also allows dealing with the nonlinear behavior of materials [57]. This paper proposes the development of a FEM-BEM coupling for the modeling of the electro-magneto-mechanically problem involving ME composites. This approach is particularly interesting since only the active domains associated with the materials need to be discretized and the free space domain is properly accounted for. In addition, a single discretization can be used for the full coupled problem.

The outline of the paper is as follows: in section 2, after introducing the full set of continuous governing equations and behavioral laws, we develop the weak and discrete forms associated with the presented coupling strategy. In section 3, we present the implemented iterative algorithm used for solving

the multiphysics problem. In section 4, the chosen application and some results of its modeling will be presented.

2. Theoretical framework of magnetoelectric coupling

In this section, the FEM-BEM coupling used to address the open boundary magnetoelectric problem is described. First, the multiphysics problem is introduced and the electro-mechanical and magneto-mechanical behavior laws are defined. The weak and discrete formulations as well as the coupling between the FEM and the BEM are finally detailed. To facilitate the reading of the following sections, the basic magnetic, electric and mechanical quantities are summarized in Table 1.

Symbol	Description	SI-unit
$\boldsymbol{u}$	Mechanical displacement	m
$\boldsymbol{f}$	Body forces	N
$\boldsymbol{S}$	Linear strain	-
$\boldsymbol{T}$	Cauchy stress	Pa
φ	Electric scalar potential	V
Q_s	Electric surface charge density	$\mathrm{C\,m^{-2}}$
$\boldsymbol{E}$	Electric field	$\mathrm{V\,m^{-1}}$
$\boldsymbol{D}$	Electric displacement	$\mathrm{C\,m^{-2}}$
ϕ_{red}	Magnetic reduced scalar potential	A
$\boldsymbol{J_s}$	Electric current density	$\mathrm{A\,m^{-2}}$
$\boldsymbol{H}$	Magnetic field	$\mathrm{A\,m^{-1}}$
$\boldsymbol{B}$	Magnetic flux density	T

Table 1: Magnetic, electric and mechanical fields and their SI-Units.

2.1. Electro-magneto-mechanical problem description

We consider a domain $\Omega \in \mathbb{R}^d$ $(d = 2, 3)$ with $\Omega = \Omega_0 \cup \Omega_{pe} \cup \Omega_{pm}$ where Ω_0, Ω_{pe} and Ω_{pm} represent the free space, the magnetostrictive and the piezoelectric domains, respectively. The magnetostrictive and the piezoelectric domains are assumed at rest and contained in the free space Ω_0 with a constant dielectric permittivity ε_0 and a constant magnetic permeability μ_0. The bond at the interface between the magnetostrictive and piezoelectric bodies is assumed to be perfect.

Considering fields of low frequency to static fields, the set of equations governing electromagnetic phenomena are given by Maxwell's equations in the frame of electrostatics and magnetostatics,

$$\boldsymbol{\nabla} \cdot \boldsymbol{B} = 0 \quad \forall \boldsymbol{x} \in \Omega, \tag{1}$$

$$\boldsymbol{\nabla} \times \boldsymbol{H} = \boldsymbol{J_s} \quad \forall \boldsymbol{x} \in \Omega, \tag{2}$$

$$\boldsymbol{\nabla} \cdot \boldsymbol{D} = 0 \quad \forall \boldsymbol{x} \in \Omega, \tag{3}$$

$$\boldsymbol{\nabla} \times \boldsymbol{E} = 0 \quad \forall \boldsymbol{x} \in \Omega, \tag{4}$$

where the electric current density $\boldsymbol{J_s}$ is taken as the input of the problem and considered null inside the active material and $\boldsymbol{\nabla}\cdot$ and $\boldsymbol{\nabla}\times$, respectively, the divergence and the rotational operators with respect to $\boldsymbol{x}$. To this set of equation, the balance of linear momentum is added to describe the mechanical equilibrium also in quasi-static fields by neglecting inertia effects:

$$\boldsymbol{\nabla} \cdot \boldsymbol{T} + \boldsymbol{f} = 0 \quad \forall \boldsymbol{x} \in \Omega_m, \tag{5}$$

where the body force $\boldsymbol{f}$ is also taken null inside the active material.

The boundary $\partial\Omega_m$ of the mechanical domain $\Omega_m = \Omega_{pe} \cup \Omega_{pm}$ is partitioned as $\partial\Omega_m = \partial\Omega_m^u \cup \partial\Omega_m^t$ with $\partial\Omega_m^u \cap \partial\Omega_m^t = \emptyset$, and the conditions for the displacements $\boldsymbol{u}^s$ and the surface tractions $\boldsymbol{f}^T$ are given by:

$$\boldsymbol{u} = \boldsymbol{u}^s \quad \forall \boldsymbol{x} \in \partial\Omega_m^u, \tag{6}$$

$$\boldsymbol{T} \cdot \boldsymbol{n} = \boldsymbol{f}^T \quad \forall \boldsymbol{x} \in \partial\Omega_m^t, \tag{7}$$

In (7), $\boldsymbol{n}$ denotes the outward unit normal vector to the surface $\partial\Omega$. Similarly, the boundary $\partial\Omega_e$ of the electrical domain Ω_e is partitioned such that $\partial\Omega_e = \partial\Omega_e^\varphi \cup \partial\Omega_e^d$ and $\partial\Omega_e^\varphi \cap \partial\Omega_e^d = \emptyset$, with the conditions for the electric potential φ^0 and the surface charge density Q_s:

$$\varphi = \varphi^0 \quad \forall \boldsymbol{x} \in \partial\Omega_e^\varphi, \tag{8}$$

$$\boldsymbol{D} \cdot \boldsymbol{n} = -Q_s \quad \forall \boldsymbol{x} \in \partial\Omega_e^d. \tag{9}$$

In a pure FEM approach, the magnetic domain contains the active materials and the free space domain Ω_0 with $\Omega = \Omega_m \cup \Omega_0$ and $\Omega_m = \Omega_{pe} \cup \Omega_{pm}$ the magnetic subdomain associated with the active materials. Its boundary $\partial\Omega_0$ would be the boundary of the air region partitioned such that

$\partial\Omega_0 = \partial\Omega_0^h \cup \partial\Omega_0^b$ and $\partial\Omega_0^h \cup \partial\Omega_0^b = \emptyset$, with the conditions for the magnetic flux density Φ_0 and the magnetic field:

$$\boldsymbol{B} \cdot \boldsymbol{n} = -\Phi_0 \quad \forall \boldsymbol{x} \in \partial\Omega_0^b \tag{10}$$

$$\boldsymbol{H} \times \boldsymbol{n} = \boldsymbol{0} \quad \forall \boldsymbol{x} \in \partial\Omega_0^h \tag{11}$$

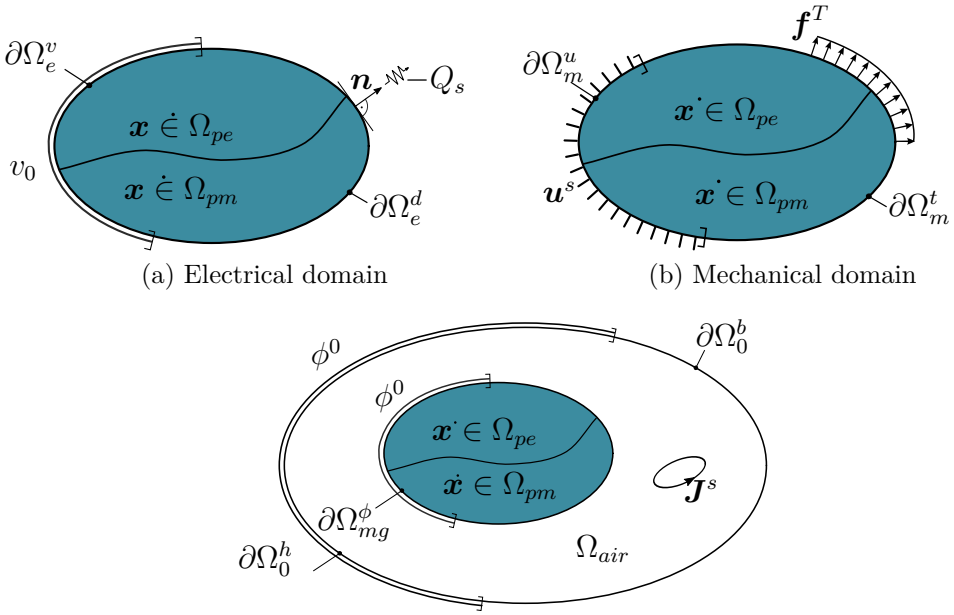

(a) Electrical domain

(b) Mechanical domain

(c) Magnetic domain

Figure 1: Representation of the study domains of the electro-magneto-mechanical problem by the FEM.

In all generality, mixed boundary conditions can be applied on $\partial\Omega_0$. However in practice, a normal magnetic field equal to zero is often imposed. In FEM, Ω_0 is supposed to approach the open infinite free space domain surrounding the physical device so clearly, for the FEM approach to be accurate for the magnetic problem, a large enough domain Ω_0 must be considered. Pure FEM formulations of the magnetoelectric effect can be found in [58] [59]. The FEM-BEM coupling does not need such approximations and the decay of magnetic fields is properly taken into account without the need of explicitly considering a free space domain.

2.2. Behavioral laws

Linear behavior laws are considered for both the electro-mechanical and the magneto-mechanical phases. Although the magneto-mechanical behavior is strongly non-linear, it is possible to describe it using a linearized piezo-magnetic behavior law [60] obtained by considering a magneto-mechanical polarization state composed by a polarizing magnetic field and a mechanical prestress and by working under conditions which respects small variations around this state. An analogous approach was applied to the linear piezo-electric behavior in [61].

Assuming the existence of a thermodynamic potential, it follows that the behavioral relations depend on the choice of state variables. In this context, despite the heterogeneous nature of the considered structures, both the piezoelectric and piezomagnetic relations can be derived from the potential (12),

$$\begin{aligned} H^{me}\left(\boldsymbol{E},\boldsymbol{H},\boldsymbol{S}\right) = \underbrace{\frac{1}{2}\boldsymbol{S}:\mathcal{C}^{\boldsymbol{E},\boldsymbol{H}}:\boldsymbol{S}}_{H^{mech}} - \underbrace{\frac{1}{2}\boldsymbol{E}\cdot\boldsymbol{\varepsilon}^{\boldsymbol{S}}\cdot\boldsymbol{E}}_{H^{diel}} - \underbrace{\frac{1}{2}\boldsymbol{H}\cdot\boldsymbol{\mu}^{\boldsymbol{S}}\cdot\boldsymbol{H}}_{H^{magn}} \\ - \underbrace{\boldsymbol{E}\cdot\mathsf{e}:\boldsymbol{S}}_{H^{piel}} - \underbrace{\boldsymbol{H}\cdot\mathsf{q}:\boldsymbol{S}}_{H^{pimg}}, \end{aligned} \tag{12}$$

where the different terms of (12) are the purely mechanical (H^{mech}), the purely dielectric (H^{diel}), the purely magnetic (H^{magn}), the piezoelectric (H^{piel}) and the piezomagnetic (H^{pimg}) energies. In (12), $\mathcal{C}$, $\boldsymbol{\varepsilon}$, $\boldsymbol{\mu}$, e and q represent the fourth-order elasticity tensor, the second-order permittivity tensor, the second-order permeability tensor, the third-order piezoelectric tensor and the third-order piezomagnetic tensor, respectively. There are derived from the potential function H^{me} as:

$$\begin{gathered} \mathcal{C} = \partial^2_{\boldsymbol{SS}} H^{me},\ \boldsymbol{\varepsilon} = \partial^2_{\boldsymbol{EE}} H^{me},\ \boldsymbol{\mu} = \partial^2_{\boldsymbol{HH}} H^{me}, \\ \mathsf{e} = \partial^2_{\boldsymbol{SE}} H^{me},\ \mathsf{q} = \partial^2_{\boldsymbol{SH}} H^{me}, \end{gathered} \tag{13}$$

The behavior relations of the linear electro-magneto-mechanical coupling are then defined by:

$$\boldsymbol{T} = -{}^{t}\mathsf{e} \cdot \boldsymbol{E} - {}^{t}\mathsf{q} \cdot \boldsymbol{H} + \mathcal{C}^{\boldsymbol{E},\boldsymbol{H}} : \boldsymbol{S}, \tag{14}$$

$$\boldsymbol{D} = \boldsymbol{\varepsilon}^{\boldsymbol{S}} \cdot \boldsymbol{E} + \mathsf{e} : \boldsymbol{S}, \tag{15}$$

$$\boldsymbol{B} = \boldsymbol{\mu}^{\boldsymbol{S}} \cdot \boldsymbol{H} + \mathsf{q} : \boldsymbol{S}, \tag{16}$$

where ${}^{t}(\bullet)$ denotes the transpose operator. In (14)–(16), the piezoelectric tensor e is taken null in the piezomagnetic phase and the piezomagnetic tensor q is taken equal to zero in the piezoelectric phase. The extrinsic nature of the strain-induced magnetoelectric effect considered here is highlighted by the absence of an eventual explicit magnetoelectric coefficient $\boldsymbol{\alpha}$ linking the electric and magnetic fields in equations (15) and (16).

2.3. Choice of resolution variables

2.3.1. Variable of the mechanical problem

The deformations brought into play by the active materials considered are relatively low. Under the small deformation hypothesis, the linear strain tensor is defined by:

$$\boldsymbol{S} = \mathrm{sym}\left(\boldsymbol{\nabla}\boldsymbol{u}\right) = \frac{1}{2}\left(\boldsymbol{\nabla}\boldsymbol{u} + {}^{t}\boldsymbol{\nabla}\boldsymbol{u}\right), \tag{17}$$

where $\boldsymbol{\nabla}$ denotes the gradient operator with respect to $\boldsymbol{x}$ and $\boldsymbol{u}$ is the mechanical displacement vector field. As $\boldsymbol{S}$ will spontaneously appear in the weak form of the mechanical problem, we chose the mechanical displacement as the solving variable of the mechanical problem.

2.3.2. Variable of the electrical problem

From (4) in the quasistatic regime, the electric field derives from a scalar potential φ,

$$\boldsymbol{E} = -\boldsymbol{\nabla}\varphi. \tag{18}$$

The computation of the electric field via the scalar electric potential φ is a standard procedure in electrostatics. It involves a state variable, the electric voltage, with a physical meaning and that can be directly imposed as a boundary condition.

2.3.3. Variable of the magnetic problem

In an approach equivalent to a Helmholtz decomposition, the magnetic field $\boldsymbol{H}$ can be decomposed into two fields (19): $\boldsymbol{H_0}$, the field created by the electric current density $\boldsymbol{J_s}$ and $\boldsymbol{H_{red}}$ the magnetic field created by the magnetized matter:

$$\boldsymbol{H} = \boldsymbol{H_0} + \boldsymbol{H_{red}}. \tag{19}$$

Assuming that all electric currents are external to the active materials, it follows that:

$$\boldsymbol{\nabla} \times \boldsymbol{H_0} = \boldsymbol{J_s}. \tag{20}$$

From (19)–(20) together with (2), we get:

$$\boldsymbol{\nabla} \times \boldsymbol{H_{red}} = 0. \tag{21}$$

Therefore, there exists a reduced scalar field ϕ_{red} such that:

$$\boldsymbol{H_{red}} = -\boldsymbol{\nabla}\phi_{red}, \tag{22}$$

with ϕ_{red} the magnetic reduced scalar potential. This potential is the independent variable of the magnetic problem. There are some clear advantages to the use of ϕ_{red} as a resolution variable than a vector potential: it leads to shape functions which are nodal/scalar quantities and their gradients are easier to compute and integrate than vector shape functions and their curl. This choice of resolution variable can however lead to cancellation errors for problems with high magnetic permeability. This is not the case for the considered magnetostrictive and piezoelectric materials [62].

2.4. Weak formulations of the electro-magneto-mechanical problem

From the mechanical and electromagnetic governing equations (1)-(5) and the behavioral laws (14)-(16) three sub-problems arise: an electrical, a mechanical and a magnetic problem which will be developed separately. Boundary value problems associated with the electrical and mechanical sub-problems are solved using the FE method while the open-boundary value problem associated with the magnetic sub-problem is solved using FEM-BEM. In the following subsections, weak formulations of the electrical and mechanical coupled sub-problems are briefly recalled and the weak formulation of the magnetic problem is given in details.

2.4.1. Weak form of the mechanical problem

Considering the coupled behavior law (14), the decomposition of the magnetic field (19) and an appropriate virtual mechanical displacement vector field $\boldsymbol{\delta u}$, which fulfills the homogeneous condition $\boldsymbol{\delta u} = \mathbf{0}$ on $\partial\Omega_m^u$, the weak formulation of the balance of linear momentum (5) is given by:

find $\boldsymbol{u}$ such that:

$$\begin{aligned} &\int_{\Omega_m} \boldsymbol{\delta S} : \mathcal{C} : \boldsymbol{S}\ d\Omega - \int_{\Omega_{pe}} \boldsymbol{\delta S} : {}^{t}\mathsf{e} \cdot \boldsymbol{E}\ d\Omega - \int_{\Omega_{pm}} \boldsymbol{\delta S} : {}^{t}\mathsf{q} \cdot \boldsymbol{H_{red}}\ d\Omega \\ &= \int_{\Omega_{pm}} \boldsymbol{\delta S} : {}^{t}\mathsf{q} \cdot \boldsymbol{H_0}\ d\Omega + \int_{\Omega_m} \boldsymbol{\delta u} \cdot \boldsymbol{f}\ d\Omega + \int_{\partial\Omega_m^t} \boldsymbol{\delta u} \cdot \boldsymbol{f}^T\ d\partial\Omega_m \quad \forall \boldsymbol{\delta u}, \end{aligned} \tag{23}$$

where, by definition, $\boldsymbol{\delta S}(\boldsymbol{x}) = \mathrm{sym}\,(\boldsymbol{\nabla \delta u}(\boldsymbol{x}))$.

2.4.2. Weak form of the electrical problem

Though a FEM-BEM approach could be used for the electric problem with the surface term that accounts for the leaks of the displacement field, for our particular application, this coupling can be avoided for two reasons. Firstly, piezoelectric materials have high electric permittivity which allow them to canalize the displacement field inside the material domain, leading to low values of the stray field. Secondly, the piezoelectric material is in contact with two electrodes which act as equipotential surface regions, each one fixing the potential in a surface region of the piezoelectric material. The boundary of the active material can then be partitioned, without much loss of accuracy, into fixed potential regions and regions with no leaks, thus making the problem well posed for a FEM approach.

Considering the coupled behavior law (15) and an appropriate virtual electric scalar potential field $\delta\varphi$, which fulfills the homogeneous condition $\delta\varphi = 0$ on $\partial\Omega_m^\varphi$, the FEM weak formulation of the Maxwell-Gauss law (3) reads:

find φ such that:

$$\int_{\Omega_m} \boldsymbol{\delta E} \cdot \boldsymbol{\varepsilon^S} \cdot \boldsymbol{E}\ d\Omega + \int_{\Omega_{pe}} \boldsymbol{\delta E} \cdot \boldsymbol{e} : \boldsymbol{S}\ d\Omega = \int_{\partial\Omega_e^d} \delta\varphi\ D_n d\partial\Omega_e \quad \forall \delta\varphi, \tag{24}$$

with $\boldsymbol{\delta E} = -\boldsymbol{\nabla}\delta\varphi$. As a reminder, the electric charge density is zero in the piezoelectric material and therefore does not appear in the formulation (24).

2.4.3. Weak form of the magnetic problem

To establish the FEM-BEM weak formulation of the magnetic problem, the magnetic domain Ω is subdivided into an open exterior Ω_0 and an interior Ω_m domains (Figure 2). The interface between the two magnetic subdomains, boundary of the active material, is denoted by $\partial\Omega_m$.

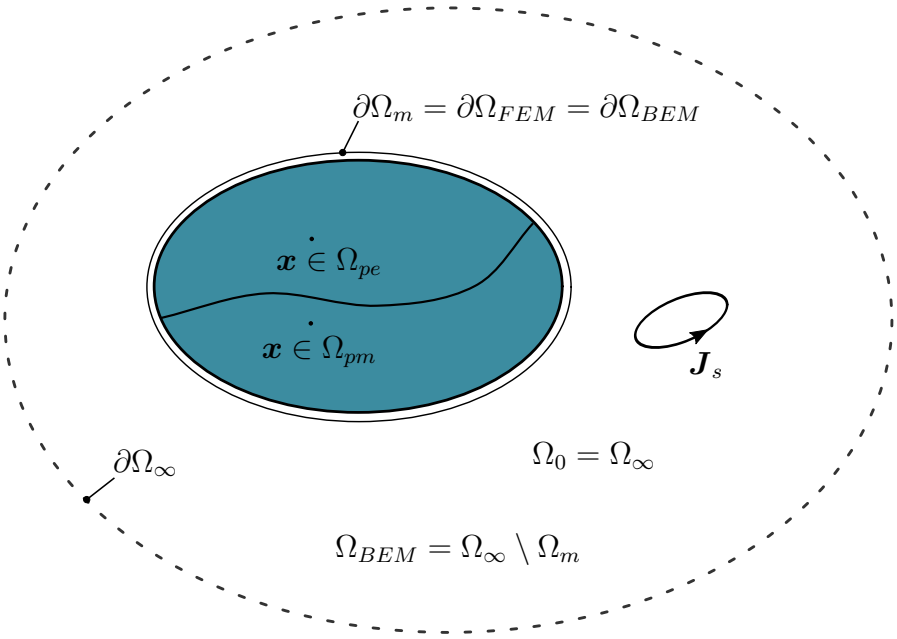

Figure 2: Sub-domains of the magnetic problem based on a FEM-BEM formulation. The FEM is associated with the bounded domain $\Omega_m = \Omega_{pe} \cup \Omega_{pm}$ and the BEM with the exterior infinite domain Ω_{BEM} corresponding to an infinite free space. The FEM and BEM are coupled on the common boundary $\partial\Omega_m$. This boundary can be fictitious but will coincide here with the boundary of magnetizable bodies Ω_m in the open domain Ω_{BEM}.

2.4.3.1. Magnetic formulation inside the active material

To obtain a magnetic formulation inside the active domain Ω_m, we consider the Maxwell-Thomson equation (1) weighted by an appropriate virtual magnetic scalar potential field $\delta\phi$ and integrated by part on the domain Ω_m:

$$\int_{\Omega_m} \boldsymbol{\nabla}\delta\phi \cdot \boldsymbol{B}\ d\Omega_m - \int_{\partial\Omega_m} \delta\phi\ B_n\ d\partial\Omega_m = 0 \quad \forall\delta\phi, \tag{25}$$

where $B_n = \boldsymbol{B} \cdot \boldsymbol{n}$ with $\boldsymbol{n}$ the unitary normal vector perpendicular to the elementary surface $d\partial\Omega_m$. Let's now replace $\boldsymbol{B}$ by the behavioral law (16) and $\boldsymbol{H}$ by the decomposition (19). This results in the weak formulation of the Gauss-Thomson law (1) in the domain Ω_m:

find (ϕ_{red}, B_n) such that:

$$\begin{aligned}\int_{\Omega_m} \boldsymbol{\nabla}\delta\phi \cdot \boldsymbol{\mu^S} \cdot \boldsymbol{\nabla}\phi_{red}\ d\Omega_m - \int_{\Omega_{pm}} \boldsymbol{\nabla}\delta\phi \cdot \boldsymbol{q} : \boldsymbol{S}\ d\Omega_m + \int_{\partial\Omega_m} \delta\phi\ B_n\ d\partial\Omega_m \\ = \int_{\Omega_m} \boldsymbol{\nabla}\delta\phi \cdot \boldsymbol{\mu^S} \cdot \boldsymbol{H_0}\ d\Omega_m \quad \forall\delta\phi.\end{aligned} \tag{26}$$

In a classical FEM approach, a sufficiently large free space domain is considered in order to neglect the surface term B_n. A FEM-BEM coupling can take into account leakage fields and thus not have to explicitly consider a free space region.

2.4.3.2. Magnetic formulation in the free space domain

Let's consider the Maxwell-Thomson equation (1). In the free space domain Ω_0 the permeability is uniform, linear and taken equal to the vacuum permeability. In this case, the outer magnetic reduced scalar potential fulfills the Laplace equation [63]:

$$\Delta\phi_{red} = 0. \tag{27}$$

Green's third identity can then be applied to ϕ_{red} on a closed surface $\partial\Omega$ contained within the free space domain Ω_0:

$$\frac{1}{2}\phi_{red} = \int_{\partial\Omega} \phi_{red}\ \frac{\partial G}{\partial n} d\partial\Omega - \int_{\partial\Omega} G\ \frac{\partial \phi_{red}}{\partial n} d\partial\Omega, \tag{28}$$

with G the Green's kernel fundamental solution of the Laplace equation defined as:

$$G(r) = \frac{1}{4\pi r} \quad (3D), \tag{29}$$

and

$$\frac{\partial \phi_{red}}{\partial n} = \boldsymbol{\nabla}\phi_{red} \cdot \boldsymbol{n}. \tag{30}$$

In order to couple fields at the interface $\partial\Omega_m$ between the active material and the free space domain, it is preferable to introduce the quantity B_n in the strong formulation. Indeed, in the free space domain, this quantity is given by:

$$B_n = \mu_0 \left((\boldsymbol{H_0} \cdot \boldsymbol{n}) - \frac{\partial \phi_{red}}{\partial n} \right), \tag{31}$$

which is equivalent to:

$$\frac{\partial \phi_{red}}{\partial n} = H_{0n} - \frac{B_n}{\mu_0}, \tag{32}$$

with $H_{0n} = \boldsymbol{H_0} \cdot \boldsymbol{n}$. Introducing this last relation into the previous strong formulation (28) we get:

$$\frac{1}{2}\phi_{red} = \int_{\partial\Omega} \frac{\partial G}{\partial n} \phi_{red} \; d\partial\Omega - \int_{\partial\Omega} G \left(H_{0n} - \frac{B_n}{\mu_0} \right) d\partial\Omega. \tag{33}$$

Rearranging the terms, the strong formulation of the magnetic problem in the free space domain becomes:

$$-\frac{1}{2}\phi_{red} + \int_{\partial\Omega} G \frac{B_n}{\mu_0} d\partial\Omega + \int_{\partial\Omega} \phi_{red} \frac{\partial G}{\partial n} d\partial\Omega = \int_{\partial\Omega} G \; H_{0n} d\partial\Omega. \tag{34}$$

As B_n and ϕ_{red} are considered continuous across $\partial\Omega_m$, the weak formulation in the free space domain can then be obtained by projecting (34) onto an appropriate virtual magnetic scalar potential field $\delta\phi_0$ associated with a closed surface $\partial\Omega$ corresponding here to the external surface $\partial\Omega_m$ of the active material domain:

Find (ϕ_{red}, B_n) such that :

$$\begin{aligned} &\int_{\partial\Omega_m} \delta\phi_0 \int_{\partial\Omega_m} \phi_{red} \frac{\partial G}{\partial n} \; d\partial\Omega_m d\partial\Omega_m + \int_{\partial\Omega_m} \delta\phi_0 \int_{\partial\Omega_m} G \frac{B_n}{\mu_0} \; d\partial\Omega_m d\partial\Omega_m \\ &- \int_{\partial\Omega_m} \delta\phi_0 \; \frac{1}{2} \; \phi_{red} \; d\partial\Omega_m = \int_{\partial\Omega_m} \delta\phi_0 \int_{\partial\Omega_m} G \; H_{0n} \; d\partial\Omega_m d\partial\Omega_m \quad \forall \delta\phi_0. \end{aligned} \tag{35}$$

Neglecting surface currents on $\partial\Omega_m$, the interface conditions for the magnetic fields along $\partial\Omega_m$ read:

$$[\ \boldsymbol{H} \times \boldsymbol{n}\ ]_{\partial\Omega_m} = 0, \tag{36}$$

$$[\ \boldsymbol{B} \cdot \boldsymbol{n}\ ]_{\partial\Omega_m} = 0, \tag{37}$$

where $[\bullet]_{\partial\Omega}$ denotes the jump across the surface $\partial\Omega_m$. Taking ϕ_{red} continuous across $\partial\Omega_m$ ensures (36). The continuity of the normal magnetic induction field across $\partial\Omega_m$, translated by (37), allows us to couple both magnetic formulations (26) and (35) which concludes the FEM-BEM coupling.

2.4.3.3. Computation of the source field

In a pure FEM approach, the source field is obtained in a pre-resolution on a mesh containing the entire computational domain. For problems with a large free space, this resolution increases the overall computational cost of the multiphysics problem. With the FEM-BEM coupling, the computation of the source field is performed by the use of the Biot & Savart law (38) which involves the integration of $\boldsymbol{\nabla} G$.

$$\boldsymbol{H_0} = \int \boldsymbol{\nabla} G \times \boldsymbol{J_s}\ d\Omega. \tag{38}$$

Hence, there will be no need to consider a free space domain to compute the source field. In addition, from a numerical resolution point of view, the computational cost of the source field at the Gauss points of the mesh of the active material will be independent of the distance between the field source and the active material domain, which could mean a huge difference in computation times.

2.5. Discrete formulations of the electro-magneto-mechanical problem

The following FEM-BEM formulations will be derived in vector-matrix notation, which results in a closed efficient description of the implementation. To do so, all vectors and matrices will be signified with an underline as $\underline{\bullet}$. In addition, for the Cauchy stress tensor and the linear strain tensor we will used Voigt's notation:

$$\underline{\boldsymbol{T}} = {}^{\mathrm{t}}(T_{11}, T_{22}, T_{33}, T_{12}, T_{23}, T_{13}) \text{ and } \underline{\boldsymbol{S}} = {}^{\mathrm{t}}(S_{11}, S_{22}, S_{33}, 2S_{12}, 2S_{23}, 2S_{13})\,. \tag{39}$$

The domain Ω is discretized into a number n_{elem} of finite elements resulting in a discrete counterpart such that: $\Omega \approx \Omega^h = \bigcup_{e=1}^{n_{elem}} \Omega_e$, where $(\bullet)^h$ indicates the approximated domain and Ω_e a finite element. The fields as well as their virtual counterparts are approximated element-wise by means of,

$$\left\{\underline{\boldsymbol{u}}^h, \underline{\boldsymbol{\delta u}}^h\right\} = \sum_{I=1}^{n_{node}} N_u^I \left\{\underline{\widetilde{\boldsymbol{u}}}^I, \underline{\widetilde{\boldsymbol{\delta u}}}^I\right\} = \underline{\boldsymbol{N}}_u^e \left\{\underline{\widetilde{\boldsymbol{u}}}^e, \underline{\widetilde{\boldsymbol{\delta u}}}^e\right\}, \tag{40}$$

$$\left\{\varphi^h, \delta\varphi^h\right\} = \sum_{I=1}^{n_{node}} N_\varphi^I \left\{\widetilde{\varphi}^I, \widetilde{\delta\varphi}^I\right\} = \underline{\boldsymbol{N}}_\varphi^e \left\{\underline{\widetilde{\boldsymbol{\varphi}}}^e, \underline{\widetilde{\boldsymbol{\delta\varphi}}}^e\right\}, \tag{41}$$

$$\left\{\phi^h, \delta\phi^h\right\} = \sum_{I=1}^{n_{node}} N_\phi^I \left\{\widetilde{\phi}^I, \widetilde{\delta\phi}^I\right\} = \underline{\boldsymbol{N}}_\phi^e \left\{\underline{\widetilde{\boldsymbol{\phi}}}^e, \underline{\widetilde{\boldsymbol{\delta\phi}}}^e\right\}, \tag{42}$$

where $\underline{\widetilde{\boldsymbol{u}}}^I$, $\widetilde{\varphi}^I$ and $\widetilde{\phi}^I$ denote, respectively, the discrete nodal displacement, the discrete nodal electric potential and the discrete nodal magnetic potential at node I, and $\underline{\widetilde{\boldsymbol{u}}}^e$, $\underline{\widetilde{\boldsymbol{\varphi}}}^e$, $\underline{\widetilde{\boldsymbol{\phi}}}^e$ are the associated element vectors of unknowns. In the same way, $\underline{\widetilde{\boldsymbol{\delta u}}}^I$, $\widetilde{\delta\varphi}^I$, $\widetilde{\delta\phi}^I$, $\underline{\widetilde{\boldsymbol{\delta u}}}^e$, $\underline{\widetilde{\boldsymbol{\delta\varphi}}}^e$ and $\underline{\widetilde{\boldsymbol{\delta\phi}}}^e$ denote the respective discrete virtual counterparts. N_u^I, N_φ^I and N_ϕ^I are shape functions associated with the node I and $\underline{\boldsymbol{N}}_\bullet^e$ the corresponding matrix of shape functions. n_{node} defines the number of nodes per element. In this framework, the mechanical strain, electrical and magnetic fields as well as their respective virtual counterparts are approximated by:

$$\left\{\underline{\boldsymbol{S}}^h, \underline{\boldsymbol{\delta S}}^h\right\} = \sum_{I=1}^{n_{node}} \mathbb{B}_u^I \left\{\underline{\widetilde{\boldsymbol{u}}}^I, \underline{\widetilde{\boldsymbol{\delta u}}}^I\right\} = \mathbb{B}_u^e \left\{\underline{\widetilde{\boldsymbol{u}}}^e, \underline{\widetilde{\boldsymbol{\delta u}}}^e\right\}, \tag{43}$$

$$\left\{\underline{\boldsymbol{E}}^h, \underline{\boldsymbol{\delta E}}^h\right\} = \sum_{I=1}^{n_{node}} \mathbb{B}_\varphi^I \left\{\widetilde{\varphi}^I, \widetilde{\delta\varphi}^I\right\} = \mathbb{B}_\varphi^e \left\{\underline{\widetilde{\boldsymbol{\varphi}}}^e, \underline{\widetilde{\boldsymbol{\delta\varphi}}}^e\right\}, \tag{44}$$

$$\left\{\underline{\boldsymbol{H}}^h, \underline{\boldsymbol{\delta H}}^h\right\} = \sum_{I=1}^{n_{node}} \mathbb{B}_\phi^I \left\{\widetilde{\phi}^I, \widetilde{\delta\phi}^I\right\} = \mathbb{B}_\phi^e \left\{\underline{\widetilde{\boldsymbol{\phi}}}^e, \underline{\widetilde{\boldsymbol{\delta\phi}}}^e\right\}, \tag{45}$$

with $\mathbb{B}_u^I$, $\mathbb{B}_\varphi^I$, $\mathbb{B}_\phi^I$, $\mathbb{B}_u^e$, $\mathbb{B}_\varphi^e$ and $\mathbb{B}_\phi^e$ the node-wise and element-wise B-matrices containing the Cartesian derivatives of the shape functions involved in the discrete form of (17), (18) and (22).

2.5.1. Discrete form of the mechanical problem

The substitution of the approximations (40)–(45) in the weak form (23) of the mechanical problem yields the following discrete form:

$$\sum_{e=1}^{n_{elem}} {}^{t}\widetilde{\underline{\boldsymbol{\delta u}}}^{e} \left\{ \underbrace{\int_{\Omega_e} {}^{t}\mathbb{B}_u^e \, \underline{\boldsymbol{C}} \, \mathbb{B}_u^e \, d\Omega_e}_{\underline{\boldsymbol{k}}_{uu}^e} \, \widetilde{\underline{\boldsymbol{u}}}^{e} + \underbrace{\int_{\Omega_e} {}^{t}\mathbb{B}_u^e \, {}^{t}\underline{\boldsymbol{e}} \, \mathbb{B}_\varphi^e \, d\Omega_e}_{\underline{\boldsymbol{k}}_{u\varphi}^e} \, \widetilde{\underline{\boldsymbol{\varphi}}}^{e} \right.$$
$$\left. + \underbrace{\int_{\Omega_e} {}^{t}\mathbb{B}_u^e \, {}^{t}\underline{\boldsymbol{q}} \, \mathbb{B}_\phi^e \, d\Omega_e}_{\underline{\boldsymbol{k}}_{u\phi}^e} \, \widetilde{\underline{\boldsymbol{\phi}}}^{e} - \underbrace{\int_{\Omega_e} {}^{t}\mathbb{B}_u^e \, {}^{t}\underline{\boldsymbol{q}} \, \underline{\boldsymbol{H_0}}^{h} \, d\Omega_e}_{\underline{\boldsymbol{sh}}_{meca}^e} \right\} = 0 \quad \forall \widetilde{\underline{\boldsymbol{\delta u}}}^{e}. \tag{46}$$

2.5.2. Discrete form of the electrical problem

In the same way, the substitution of approximations in the weak form (24) of the electrical problem yields its discrete representation:

$$\sum_{e=1}^{n_{elem}} {}^{t}\widetilde{\underline{\boldsymbol{\delta\varphi}}}^{e} \left\{ \underbrace{\int_{\Omega_e} {}^{t}\mathbb{B}_\varphi^e \, \underline{\boldsymbol{\varepsilon}}^{S} \, \mathbb{B}_\varphi^e \, d\Omega_e}_{\underline{\boldsymbol{k}}_{\varphi\varphi}^e} \, \widetilde{\underline{\boldsymbol{\varphi}}}^{e} - \underbrace{\int_{\Omega_e} {}^{t}\mathbb{B}_\varphi^e \, \underline{\boldsymbol{e}} \, \mathbb{B}_u^e \, d\Omega_e}_{\underline{\boldsymbol{k}}_{\varphi u}^e} \, \widetilde{\underline{\boldsymbol{u}}}^{e} \right\} = 0 \quad \forall \widetilde{\underline{\boldsymbol{\delta\varphi}}}^{e}. \tag{47}$$

2.5.3. Discrete form of the magnetic problem

The reduced magnetic scalar potential and the linear strain vector in the weak formulation (26) are discretized using (42) and (43). For the boundary term, from the discrete point of view it is the set composed by the restriction to the facets belonging to $\partial\Omega^h$ of the elements used for the discretization of Ω^h.

The interpolation of the reduced magnetic scalar potential is thus realized by the $\hat{N}_\phi$ shape functions associated to the restriction to the boundary of the N_ϕ shape functions of the elements of Ω^h. Similarly for the normal component B_n of the magnetic induction field, which, given the continuity condition, is interpolated by 0-order shape functions $\hat{N}_0$.

$$\sum_{e=1}^{n_{elem}} {}^{\mathrm{t}}\widetilde{\underline{\boldsymbol{\delta\phi}}}^{e} \left\{ \underbrace{\int_{\Omega_e} {}^{\mathrm{t}}\mathbb{B}_{\phi}^{e}\ \underline{\boldsymbol{\mu}}^{S}\ \mathbb{B}_{\phi}^{e}\ d\Omega_e}_{\underline{\boldsymbol{k}}_{\phi\phi}^{e}}\ \widetilde{\underline{\boldsymbol{\phi}}}_{red}^{e} - \underbrace{\int_{\Omega_e} {}^{\mathrm{t}}\mathbb{B}_{\phi}^{e}\ \underline{\boldsymbol{q}}\ \mathbb{B}_{u}^{e}\ d\Omega_e}_{\underline{\boldsymbol{k}}_{\phi u}^{e}}\ \widetilde{\underline{\boldsymbol{u}}}^{e} \right.$$
$$\left. - \underbrace{\int_{\Omega_e} {}^{\mathrm{t}}\mathbb{B}_{\phi}^{e}\ \underline{\boldsymbol{\mu}}^{S}\ \underline{\boldsymbol{H_0}}^{h}\ d\Omega_e}_{\underline{\boldsymbol{sh}}_{mag}^{\Omega_m\ e}} \right\} + \sum_{e_f=1}^{n_{elem}^{f}} {}^{\mathrm{t}}\widetilde{\underline{\boldsymbol{\delta\phi}}}^{e_f} \underbrace{\int_{\partial\Omega_e} {}^{\mathrm{t}}\underline{\hat{\boldsymbol{N}}}_{\phi}^{e_f}\ \underline{\hat{\boldsymbol{N}}}_{0}^{e_f}\, d\partial\Omega_e}_{\underline{\boldsymbol{k}}_{\phi b_n}^{e f}}\ \widetilde{\underline{\boldsymbol{B_n}}}^{e_f} = 0 \quad \forall \widetilde{\underline{\boldsymbol{\delta\phi}}}^{e}, \tag{48}$$

with n_{elem}^{f} the number of facet elements belonging to $\partial\Omega^h$. The discretization of the BEM weak form (35) from the BEM formulation is performed with the same shape functions restricted to the boundary $\partial\Omega^h$:

$$\sum_{e_f=1}^{n_{elem}^{f}} {}^{\mathrm{t}}\widetilde{\underline{\boldsymbol{\delta\phi}}}_{0}^{e_f} \left\{ \underbrace{\int_{\partial\Omega_m} {}^{\mathrm{t}}\underline{\hat{\boldsymbol{N}}}_{0}^{e_f} \int_{\partial\Omega_m} \frac{\partial G}{\partial n}\ \underline{\hat{\boldsymbol{N}}}_{0}^{e_f}\ d\partial\Omega\ d\partial\Omega - \frac{1}{2}\int_{\partial\Omega_m} {}^{\mathrm{t}}\underline{\hat{\boldsymbol{N}}}_{0}^{e_f}\, \underline{\hat{\boldsymbol{N}}}_{0}^{e_f}\ d\partial\Omega}_{\underline{\boldsymbol{k}}_{\boldsymbol{\nabla_n} G}^{e f}}\ \widetilde{\underline{\boldsymbol{\phi}}}_{red}^{e_f} \right.$$
$$\underbrace{\int_{\partial\Omega_m} {}^{\mathrm{t}}\underline{\hat{\boldsymbol{N}}}_{0}^{e_f} \int_{\partial\Omega_m} \frac{G}{\mu_0}\ \underline{\hat{\boldsymbol{N}}}_{0}^{e_f}\ d\partial\Omega\ d\partial\Omega}_{\underline{\boldsymbol{k}}_{G}^{e f}}\ \widetilde{\underline{\boldsymbol{B_n}}}^{e_f}$$
$$\left. \underbrace{- \int_{\partial\Omega} {}^{\mathrm{t}}\underline{\hat{\boldsymbol{N}}}_{0}^{e_f} \int_{\partial\Omega_m} G\ H_{0_n}^{e_f}\ d\partial\Omega\ d\partial\Omega}_{\underline{\boldsymbol{sh}}_{mag}^{\partial\Omega_m\, e_f}} \right\} = 0 \quad \forall \widetilde{\underline{\boldsymbol{\delta\phi}}}^{e_f}. \tag{49}$$

Contrary to the discrete formulations (46)–(48) where local interaction between elements translates into sparse matrices, the discretisation (49) of the BEM formulation results into full matrices due to the double integration on all surface elements.

3. Iterative multiphysics resolution of the block matrix assembly

A standard assembly procedure of the element matrix $\underline{\boldsymbol{k}}_{\bullet}^{e}$ and the element right-hand side $\underline{\boldsymbol{sh}}_{\bullet}^{e}$ is applied to (46)–(49) to generate the global matrix and right-hand side:

$$\underline{\boldsymbol{K}}_{\bullet} = \bigcup_{e=1}^{n_{elem}} \underline{\boldsymbol{k}}_{\bullet}^{e} \qquad \text{and} \qquad \underline{\boldsymbol{Sh}}_{\bullet} = \bigcup_{e=1}^{n_{elem}} \underline{\boldsymbol{sh}}_{\bullet}^{e}, \tag{50}$$

where $\bigcup_{e=1}^{n_{elem}}$ is an appropriate assembly operators. The two magnetic equations are treated as block and the fully coupled problem is made of a 3×3 block of matrices representing the magnetic, the mechanical and the electrical problems. The resulting assembled matrix system is presented in equation (51) where single-physics matrices are in represented in color, sparse matrices are represented in light colors whereas full matrices are represented in dark colors.

$$\begin{bmatrix} \underline{\boldsymbol{K}}_{\phi\phi} & \underline{\boldsymbol{0}} & \underline{\boldsymbol{K}}_{\phi u} & \underline{\boldsymbol{0}} \\ & \underline{\boldsymbol{K}}_{\phi b_n} & & \\ \underline{\boldsymbol{0}} & \underline{\boldsymbol{K}}_{\nabla_{\boldsymbol{n}} G} \quad \underline{\boldsymbol{K}}_{G} & \underline{\boldsymbol{0}} & \\ \underline{\boldsymbol{K}}_{u\phi} & \underline{\boldsymbol{0}} & \underline{\boldsymbol{K}}_{uu} & \underline{\boldsymbol{K}}_{u\varphi} \\ \underline{\boldsymbol{0}} & & \underline{\boldsymbol{K}}_{\varphi u} & \underline{\boldsymbol{K}}_{\varphi\varphi} \end{bmatrix} \begin{pmatrix} \widetilde{\underline{\boldsymbol{\phi}}}_{red} \\ \widetilde{\underline{\boldsymbol{B_n}}} \\ \widetilde{\underline{\boldsymbol{u}}} \\ \widetilde{\underline{\boldsymbol{\varphi}}} \end{pmatrix} = \begin{pmatrix} \underline{\boldsymbol{Sh}}_{mag}^{\Omega_m} \\ \underline{\boldsymbol{Sh}}_{mag}^{\partial\Omega_m} \\ \underline{\boldsymbol{Sh}}_{meca} \\ \underline{\boldsymbol{Sh}}_{elec} \end{pmatrix} \tag{51}$$

This overall matrix system is not easy to solve using a single solver. Indeed, the full system is not symmetric and is made of both sparse (FEM) and full (BEM) matrices. While direct solvers are adapted for solving sparse matrix systems, iterative solvers are better suited for solving full systems. Additionally, there is a large scaling difference between coupling coefficients of the matrix $\underline{\boldsymbol{K}}_{\bullet}$. Indeed, elements of the stiffness matrix are computed using coefficients of the stiffness tensor of the order of 10-100 GPa, whereas the electric permittivity and magnetic permeability used to generate the electric and magnetic blocks are of the order of 10^{-8} F/m and 10^{-6} H/m, respectively. This difference in coupling coefficients translates into a big

difference of eigenvalues of the global matrix $\underline{\boldsymbol{K}}_{\bullet}$, and therefore in a poor conditioning number of this matrix.

To overcome these problems we implemented a block Gauss-Seidel scheme where the resolution of the global coupled system is treated as the resolution of a set of sub-problems [64] [65]. As the global matrix of each sub-system is a diagonal block of the global matrix, they are equivalent to mono-physic problems. The coupling is then introduced via the second hand term. The sub-system to be solved is given by equation (52):

$$[\underline{\boldsymbol{K}}_{ii}]\ \{\widetilde{\underline{\boldsymbol{x}}}_i^{n+1}\} = \{\underline{\boldsymbol{Sh}}_i\} - \sum_{j}^{i-1}[\underline{\boldsymbol{K}}_{ij}]\ \{\widetilde{\underline{\boldsymbol{x}}}_j^{n+1}\} - \sum_{i+1}^{n}[\underline{\boldsymbol{K}}_{ij}]\ \{\widetilde{\underline{\boldsymbol{x}}}_j^{n}\} \tag{52}$$

where $[\underline{\boldsymbol{K}}_{ii}]$ relates to mono-physic matrices, $[\underline{\boldsymbol{K}}_{ij}]$ to coupling matrices and $\{\widetilde{\underline{\boldsymbol{x}}}_i^{n+1}\}$ to the solution at step $n+1$ of the block Gauss-Seidel algorithm of the sub-system i. To solve each subsystem, a dedicated solver is used depending on the nature of the sub-problem to be solved. MUMPS direct solvers [66] are used for the FE sub-problems associated with sparse matrices, with the LU decomposition performed once and for all at the beginning of the iterative resolution. The single-physics iterations for these problems will therefore be fast. The magnetic problem is associated with full matrix blocks and more delicate to solve. Direct solvers are prohibitive in terms of computing time and iterative solvers such as GMRES are therefore preferred. The use of a block preconditioner such as the incomplete LU (ILU) preconditioner with a shift of the diagonal for the FE block and the Jacobi preconditioner possibly combined with the matrix compression for the BEM block allows to accelerate the convergence rate. If a non-linear law $\mu(H)$ is considered, then a Newton-Raphson type solver for the magnetic problem can be easily integrated in the global resolution loop.

4. Validations and Results

4.1. Validation of the purely magnetic formulation

Firstly, we validated the magnetostatic formulation considering a magnetic sphere of radius of 1 mm. The analytical solution for the magnetization of a sphere of uniform relative permeability μ_r under an uniform exciting field $\boldsymbol{H_0}$ is uniform and given by [67]:

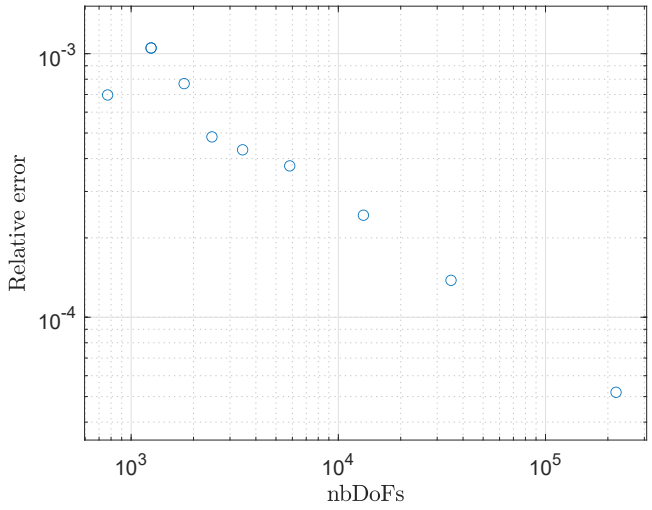

Figure 3: Relative error of the average magnetic field $\boldsymbol{H}$ as a function of the number of DoFs of the discretized problem.

$$\boldsymbol{H}_{exact} = \frac{3\ \boldsymbol{H_0}}{\mu_r + 2}. \tag{53}$$

Taking $\mu_r = 10$ and $H_0 = 50$ kAm^{-1} along the z-axis, the resulting magnetic field is also oriented along the z-direction, uniform and equal to $H = 12.5$ kAm^{-1}. Figure 3 shows the relative error,

$$\varepsilon_{\text{rel}} = \frac{\overline{\|\boldsymbol{H}^{\text{FEM-BEM}}\|} - H_{exact}}{H_{exact}} \tag{54}$$

between the average of the L^2 norm of the FEM-BEM solution $\overline{\|\boldsymbol{H}^{\text{FEM-BEM}}\|}$ and the analytical solution H_{exact} as a function of the degrees of freedom (DoFs). With a mesh of 219,014 degrees of freedom (DoFs) we obtained an average field of $12,499$ Am^{-1} clearly showing that the FEM-BEM magnetostatic formulation is very accurate.

4.2. Validation of the magneto-mechanical coupling

To validate the magneto-mechanical formulation, we considered an unconstrained magnetostrictive sphere with a constant permeability μ_r under

a uniform magnetic field and neglect the magnetic forces. Once again, the analytical magnetic field is given by (53). Defining the relative magnetic permeability μ_r as the ratio between $\boldsymbol{H}$ and $\boldsymbol{B}$ (i.e., $\mu_r = \boldsymbol{B}/(\mu_0 \boldsymbol{H})$), we obtain the following system of equations used to obtain the analytical solution:

$$\boldsymbol{T} = \mathcal{C} : \boldsymbol{S} - \mathsf{q}^t \cdot \boldsymbol{H} = \boldsymbol{0}, \tag{55}$$

$$(2\mu_0 + \mu^S)\ \boldsymbol{H} + \mathsf{q} : \boldsymbol{S} = 3\mu_0\ \boldsymbol{H_0}. \tag{56}$$

Using material parameters of Table 2 and coupling tensor structure from [68], we compare analytical results to results of FEM-BEM with increasingly finely meshed spheres and obtained the curves of Figure 4. The magnetic and mechanic problems were solved using GMRES which can handle singular systems resulting from the imposition of the Neumann conditions on the entire boundary of the mechanical problem. The tolerance of the mechanical solver was set to be 10^{-7} which is sufficient given that the averaged discrete solution shows a relative error with respect to the analytical solution greater than 10^{-5}. All the multiphysics resolutions took 6 iterations to get a convergence of the block Gauss-Seidel algorithm inferior to 10^{-6} for each single-physics solution and 8 iterations to get a tolerance of 10^{-10}, and this despite the tolerance of the discretized mechanical problem being 10^{-7}. Figure 5 shows the relative error of the magnetic and mechanical problems as the function of the iteration number of the block Gauss-Seidel algorithm for the case of of the most finely meshed sphere. At each block Gauss-Seidel iteration, the magnetic problem was solved first followed by the mechanical problem.

4.3. Simplified analytical solution

To validate the fully coupled problem, we consider a composite structure made of a piezoelectric layer poled along the z-direction sandwiched between two electrodes, a reference electrode at potential $0\,V$ and a floating one that carries the charges and outputs the voltage resulting from the deformation of the piezoelectric layer. On top and on bottom of the piezoelectric phase, two layers of magnetostrictive materials poled along the x-direction drive the deformation of the piezoelectric layer. The diagram of the geometry used in the 3D simulations is given in Figure 6.

The system works as follows : the source field $\boldsymbol{H_0}$ produces the elongation of the magnetostrictive phase which transmits the mechanical deformation

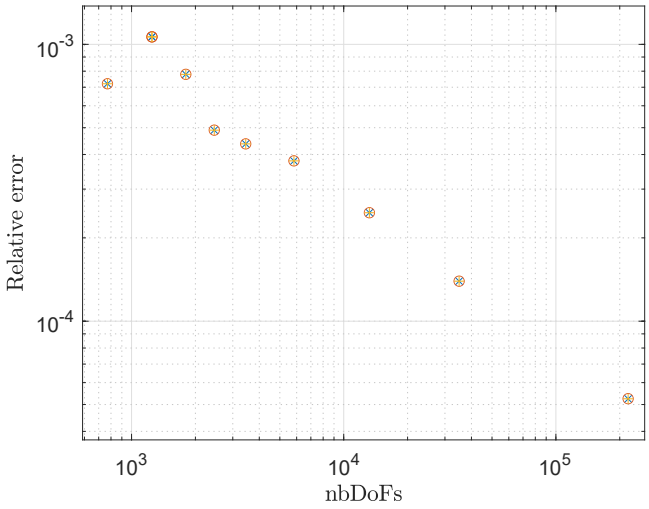

Figure 4: Relative error of the average of H, S_{11} and S_{33} as function of the number of degrees of freedom of the discretized problem.

Parameter	Value
Young modulus (GPa)	100
Poisson coefficient	0.3
q_{13} ($\mathrm{N\,A^{-1}\,m^{-1}}$)	-30
q_{33} ($\mathrm{N\,A^{-1}\,m^{-1}}$)	200
q_{24} ($\mathrm{N\,A^{-1}\,m^{-1}}$)	60
q_{15} ($\mathrm{N\,A^{-1}\,m^{-1}}$)	150
H_0 ($\mathrm{A\ m^{-1}}$)	$50 \cdot 10^3$
μ_r	10

Table 2: Material paramaters used for the modeling of the piezomagnetic sphere.

Parameter	H ($\mathrm{kA\ m^{-1}}$)	S_{11}	S_{22}	S_{33}
Value	12.110	$9.810 \cdot 10^{-6}$	$9.810 \cdot 10^{-6}$	$2.640 \cdot 10^{-5}$

Table 3: Values of the magnetic field and of the components of the strain obtained from the analytical solution.

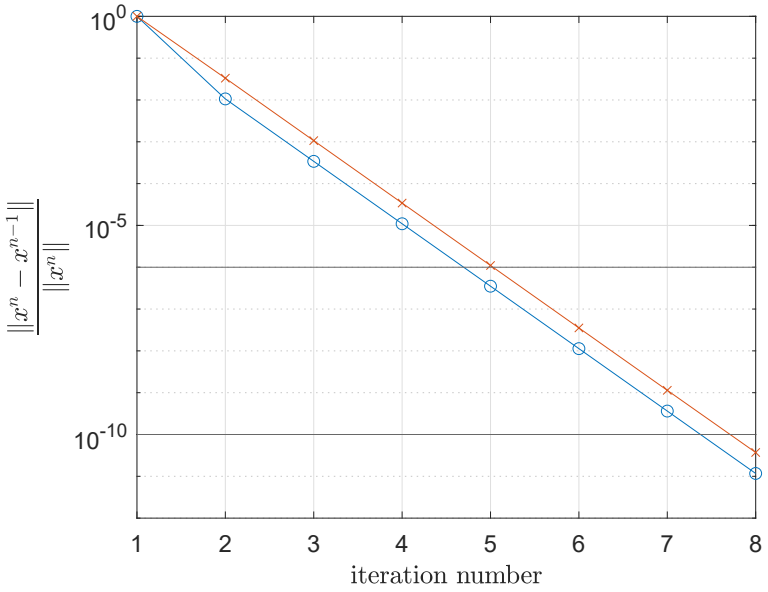

Figure 5: Convergence of magnetic (o) and mechanical (x) solutions versus iteration number of the block Gauss-Seidel algorithm.

to the piezoelectric phase thanks to the bonding between these two phases and the poling direction of the piezoelectric phase. A voltage then appears on the floating electrodes.

We compare FEM-BEM results to an analytical solution obtained with the same asumptions as in [69] but with a different set of state variables, i.e. the same strain in the piezoelectric and piezomagnetic phases, zero strain along the z-axis, zero electric field along the z-direction inside the piezoelectric phase and zero current between electrodes, which corresponds to relations (57).

$$\begin{cases} T_{11}^m = -\gamma T_{11}^e, \\ T_{22}^m = -\gamma T_{22}^e, \\ S_{11}^m = S_{11}^e, \\ S_{22}^m = S_{22}^e, \\ V_{out} = -d\ E_3^e, \end{cases} \tag{57}$$

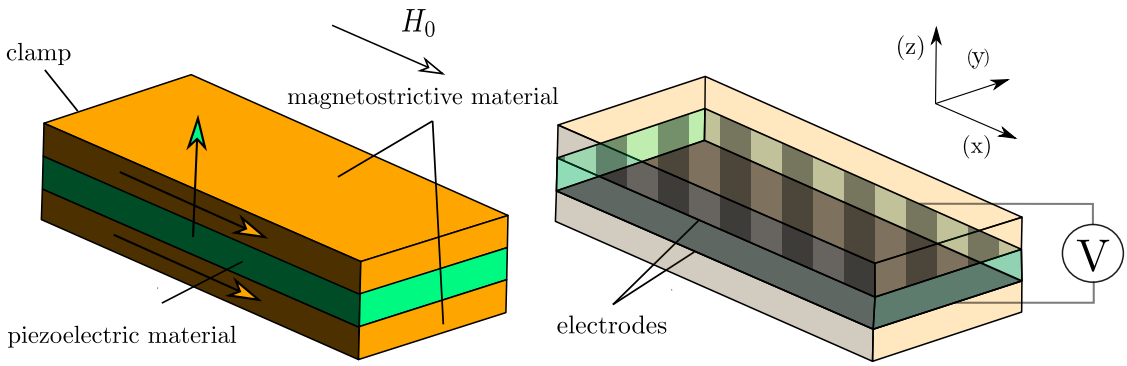

Figure 6: Diagram of the composite structure ($3 \times 6 \times 14$ mm)

where $d = 1$mm is the thickness of the piezoelectric layer, and $\gamma = 1/3$ the volume fraction of the piezoelectric layer. We will solve this set of equations together with the previously discussed but rewritten behavioral laws:

$$\begin{cases} T_{11}^e = C_{11}^E S_{11}^e + C_{12}^E S_{22}^e - e_{31} E_3, \\ T_{22}^e = C_{12}^E S_{11}^e + C_{22}^E S_{22}^e - e_{31} E_3, \\ D_3 = e_{31} S_{11}^e + e31 S_{22}^e + \varepsilon_{33} E_3, \end{cases} \\ \begin{cases} T_{11}^m = C_{11}^m S_{11}^m + C_{12}^m S_{22}^m - h_{11} H_1, \\ T_{22}^m = C_{12}^m S_{11}^m + C_{22}^m S_{22}^m - h_{12} H_1, \\ B_1 = h_{11} S_{11}^m + h_{12} S_{22}^m + \mu_{11} H_1^m \end{cases} \tag{58}$$

where the superscript $\bullet^m$ refers to the value of fields inside the magnetostrictive phase and $\bullet^e$ inside the piezoelectric phase. The solution to these equations is:

$$V_{out} = e_{31} \frac{q_{12} + q_{11}}{d\ \varepsilon_{33}\ (C_{11}^H + \gamma\, C_{11}^E + C_{12}^H + \gamma\, C_{12}^E) + 2e_{31}^2} H_1 \tag{59}$$

In order to compare this analytical solution to our simulations, we considered isotropic materials and the same mechanical properties for both the piezoelectric and magnetostrictive materials. We also didn't take into account demagnetizing fields, i.e $H_1 = H_0$ which we took from 100 Am^{-1} to 100 kAm^{-1}, while not exact, this is an acceptable approximation for materials with low relative permeability.

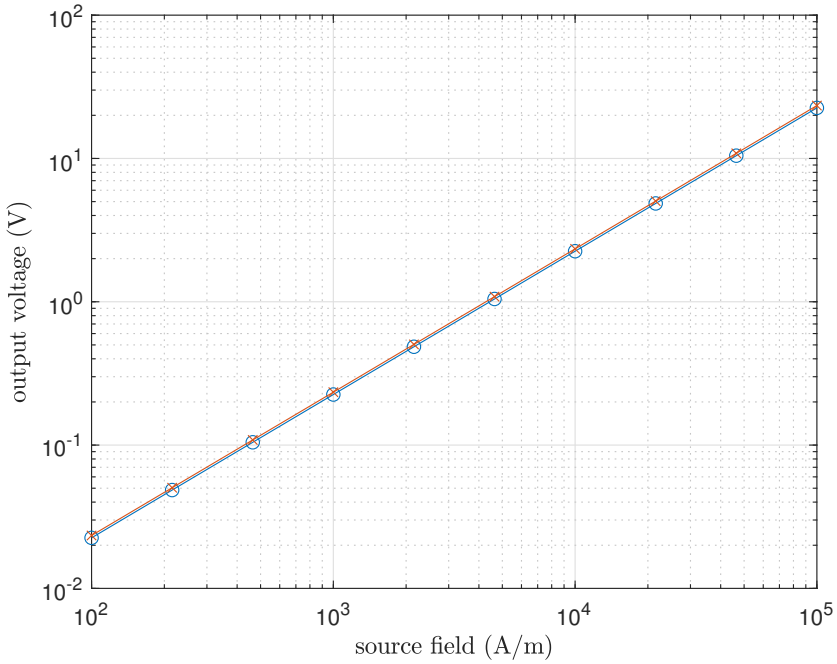

Figure 7: Output voltage of the magnetoelectric composite versus source field. (x) corresponds to the analytical solution and (o) to the simulation results.

For simulations to be closer to the conditions of the analytical solution, we assume all the coefficients in the piezoelectric and piezomagnetic tensors to be null except of those appearing in equation (59), the coefficients used are presented in Table 4. Although close to the coefficients of PZT-5A and Terfenol-D, these coefficients are not expected to be accurate but to allow us to roughly validate our formulation. The slope of the curve in Figure 7 represents the DC magnetoelectric coefficient, or the output voltage divided by the exciting magnetic field, its value is presented in Table 5. For the analytic case, it is given by:

$$\alpha = \frac{V_{out}}{H_0} = e_{31} \frac{q_{12} + q_{11}}{d\ \varepsilon_{33}(C_{11}^H + \gamma C_{11}^E + C_{12}^H + \gamma C_{12}^E) + 2e_{31}^2} \tag{60}$$

Because of demagnetizing fields, the total field inside the magnetoelectric is lower than the source field ($\mu_r > 1$). So, in theory, supposing $H_1 = H_0$ overestimates the value of the output voltage and supposing equal strain in

Parameter	Value
Young modulus (GPa)	70.3
Poisson coefficient	0.345
e_{31} (C m^{-2})	-5
q_{11} (N A^{-1} m^{-1})	200
q_{12} (N A^{-1} m^{-1})	-30
relative ε_{33} (piezoelectric layer)	1800
relative ε_{33} (piezomagnetic layer)	1
μ_r (piezoelectric layer)	5
μ_r (piezomagnetic layer)	9.3

Table 4: Coefficients used for the comparison between simulation and the analytical solution

Analytical solution	2.3397e-04 Vm/A
Simulation	2.2530e-04 Vm/A

Table 5: Comparison of magnetoelectric coefficients between simulation and analytical solution

both piezoelectric and piezomagnetic phases also overestimates the output voltage. Indeed, in the simulations it is the magnetic field which drives the deformation of the piezoelectric phase. Also, the 3D nature of the simulation (and therefore of the strain) versus the 2D strain hypothesis of the analytical formula also means that the output voltage of the fully modelled magnetoelectric should be lower than the analytical formula. A factor contributing to the high value of the output voltage of the magnetoelectric with respect to the analytical solution is edge effects due to perfect corners in our geometry and linear material laws in our simulation. Otherwise, we see very good agreement between both solutions. The magnetic, electric and mechanical solutions resulting from FEM-BEM simulations are presented in Figure 8, we see the deformation of the magnetostrictive phase, the deformation of the piezoelectric phase and the electric field appearing between the electrodes.

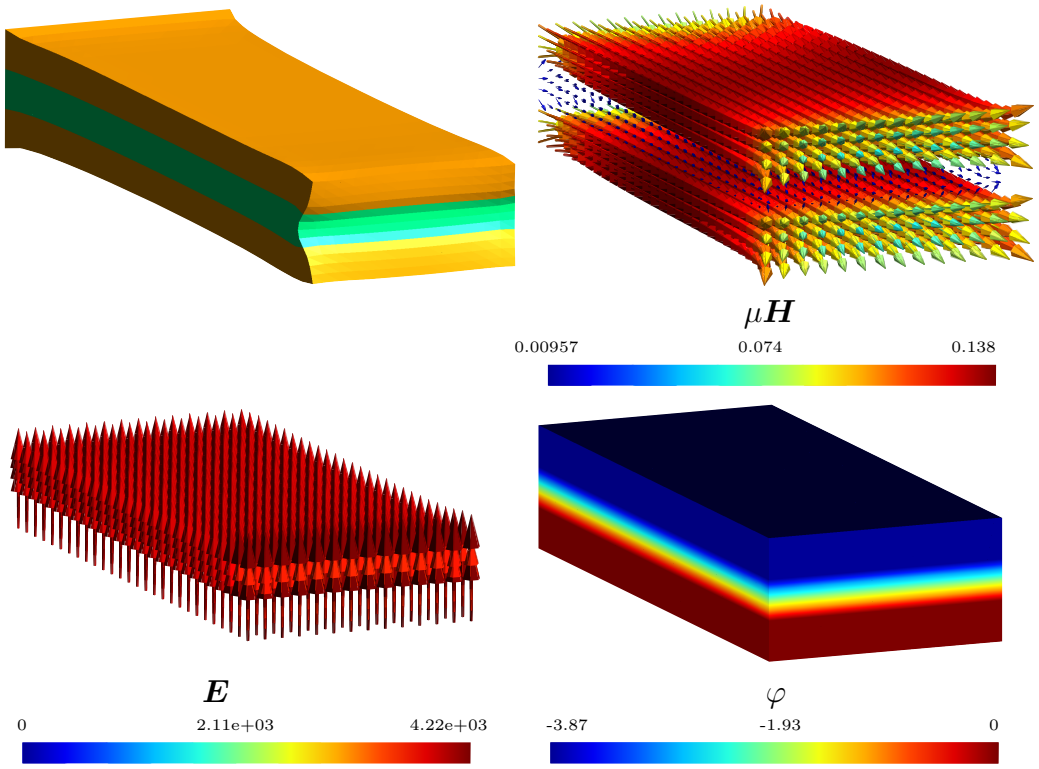

Figure 8: Three-dimensional multiphysics solutions, $\mu \boldsymbol{H}$ (T), $\boldsymbol{E}$ (V m^{-1}), φ (V

5. ME composite in an inhomogeneous field - Results

Finally we study the magnetoelectric composite structure shown in Figure 9 and fed by a volume inductor with coefficients from [68]. The coil was purposely placed in such a way that the source field seen by the composite has no symmetries and cannot be approximated by a uniform field. The considered inductor has the following dimensions: a height of 2 mm, an inner radius of 7 mm and an outer radius of 9 mm. The total current flowing though the inductor was set to 100 A. The magnetostrictive phase is considered non-linear magnetic with the relative permeability at the origin equal 100 and a saturation value of $1\,T$. We use MUMPS to solve the mechanical and the electrical problems. We also use a Newton-Raphson scheme with a tolerance of 10^{-10} for the nonlinear magnetic problem, with GMRES for solving the resulting linearized system at each nonlinear iteration. The con-

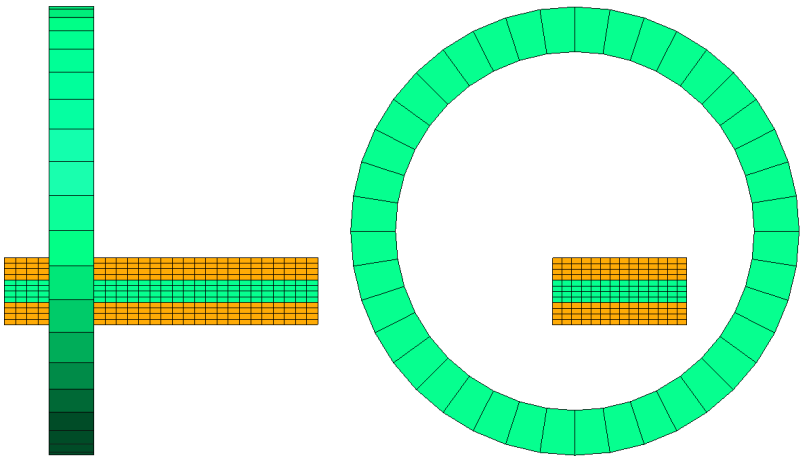

Figure 9: The studied device is made of a coil conductor around the previously described composite structure.

vergence of the magnetic problem was always achieved after two iterations of the Newton-Raphson. The stopping criteria of the Gauss-Seidel loop was set to relative 10^{-10} difference between successive solutions. Within each Gauss-Seidel iteration, the magnetic problem was solved first followed by the mechanical and the electrical problems. The convergence rate of individual single-physics problems is presented in Figure 10.

In Figure 10, from the 1^{st} to the 4^{th} iterations, we observe different convergence rates and beyond the 4^{th}, the rate of convergence is the same for all the single-physics problems. After 15 iterations, the relative convergence of 10^{-10} is achieved. In this particular test, the output voltage of the magnetoelectric is of $-0.277\,\text{V}$.

6. Conclusion

In this paper, we proposed a FEM-BEM coupling strategy for the description of 3D magnetoelectric effects in composite structures. This coupling of numerical method allowed us only not to explicitly consider a free space domain, and thus to use a single mesh for the three subproblems. We validated our magnetostatic and magneto-mechanical formulation against analytical solutions, and we compared the results of our full coupled problem against a rough analytical solution with good agreement. We also tested the presented

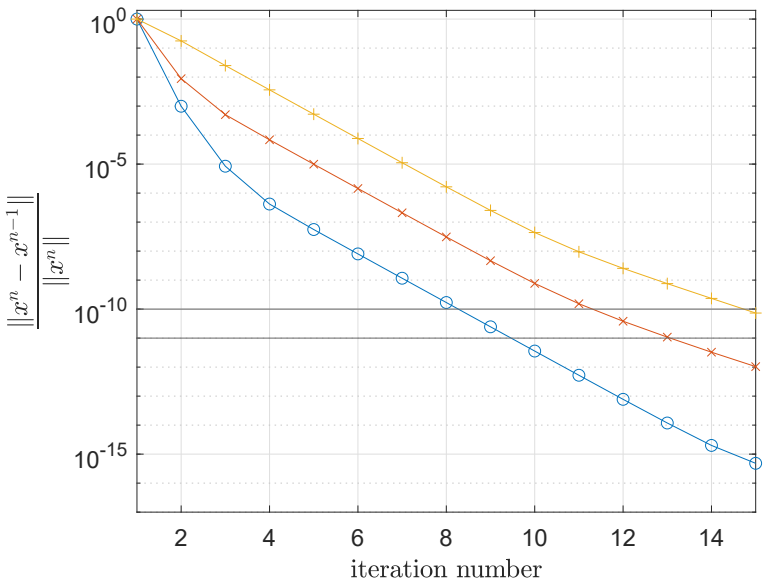

Figure 10: Convergence of magnetic (o), mechanical (x) and electric (+) solutions vs iteration number of the block Gauss-Seidel algorithm.

full formulation of the magnetoelectric composite structure on a three layer device driven by a coil, with a non-linear material law for the magnetostrictive material and explored the performance of the block Gauss-Seidel algorithm for solving multiphysics problems in the previously described situation.

Acknowledgment

This work is supported by the Centre National de la Recherche Scientifique (CNRS) and the Université Grenoble Alpes, France.

References

[1] W. Eerenstein, N. D. Mathur, J. F. Scott, Multiferroic and magnetoelectric materials, Nature 442 (2006) 759–765. URL: `https://doi.org/10.1038/nature05023`. doi:10.1038/nature05023.

[2] X. Liang, A. Matyushov, P. Hayes, V. Schell, C. Dong, H. Chen, Y. He, A. Will-Cole, E. Quandt, P. Martins, J. McCord, M. Medarde,

S. Lanceros-Méndez, S. van Dijken, N. X. Sun, J. Sort, Roadmap on magnetoelectric materials and devices, IEEE Transactions on Magnetics 57 (2021) 1–57. doi:10.1109/TMAG.2021.3086635.

[3] Y. Cheng, B. Peng, Z. Hu, Z. Zhou, M. Liu, Recent development and status of magnetoelectric materials and devices, Physics Letters A 382 (2018) 3018–3025. URL: https://www.sciencedirect.com/science/article/pii/S0375960118307394. doi:https://doi.org/10.1016/j.physleta.2018.07.014.

[4] C. Dong, Y. He, M. Li, C. Tu, Z. Chu, X. Liang, H. Chen, Y. Wei, M. Zaeimbashi, X. Wang, H. Lin, Y. Gao, N. X. Sun, A portable very low frequency (vlf) communication system based on acoustically actuated magnetoelectric antennas, IEEE Antennas and Wireless Propagation Letters 19 (2020) 398–402. doi:10.1109/LAWP.2020.2968604.

[5] C. M. Leung, X. Zhuang, D. Friedrichs, J. Li, R. W. Erickson, V. Laletin, M. Popov, G. Srinivasan, D. Viehland, Highly efficient solid state magnetoelectric gyrators, Applied Physics Letters 111 (2017) 122904. URL: https://doi.org/10.1063/1.4996242. doi:10.1063/1.4996242. arXiv:https://doi.org/10.1063/1.4996242.

[6] T. Lafont, L. Gimeno, J. Delamare, G. A. Lebedev, D. I. Zakharov, B. Viala, O. Cugat, N. Galopin, L. Garbuio, O. Geoffroy, Magnetostrictive–piezoelectric composite structures for energy harvesting, Journal of Micromechanics and Microengineering 22 (2012) 094009. URL: https://doi.org/10.1088/0960-1317/22/9/094009. doi:10.1088/0960-1317/22/9/094009.

[7] C.-W. Nan, M. I. Bichurin, S. Dong, D. Viehland, G. Srinivasan, Multiferroic magnetoelectric composites: Historical perspective, status, and future directions, Journal of Applied Physics 103 (2008) 031101. URL: https://doi.org/10.1063/1.2836410. doi:10.1063/1.2836410. arXiv:https://doi.org/10.1063/1.2836410.

[8] J. F. Scott, Multiferroic memories, Nature Materials 6 (2007) 256–257. URL: https://doi.org/10.1038/nmat1868. doi:10.1038/nmat1868.

[9] S. Kopyl, R. Surmenev, M. Surmeneva, Y. Fetisov, A. Kholkin, Magnetoelectric effect: principles and applications in biology and

medicine– a review, Materials Today Bio 12 (2021) 100149. URL: https://www.sciencedirect.com/science/article/pii/S2590006421000570. doi:https://doi.org/10.1016/j.mtbio.2021.100149.

[10] J. A. Mundy, C. M. Brooks, M. E. Holtz, J. A. Moyer, H. Das, A. F. Rébola, J. T. Heron, J. D. Clarkson, S. M. Disseler, Z. Liu, A. Farhan, R. Held, R. Hovden, E. Padgett, Q. Mao, H. Paik, R. Misra, L. F. Kourkoutis, E. Arenholz, A. Scholl, J. A. Borchers, W. D. Ratcliff, R. Ramesh, C. J. Fennie, P. Schiffer, D. A. Muller, D. G. Schlom, Atomically engineered ferroic layers yield a room-temperature magnetoelectric multiferroic, Nature 537 (2016) 523–527. URL: https://doi.org/10.1038/nature19343. doi:10.1038/nature19343.

[11] D. N. Astrov, Magnetoelectric effect in chromium oxide, Journal of Experimental and Theoretical Physics 13 (1961) 729–733.

[12] C. A. F. Vaz, J. Hoffman, C. H. Ahn, R. Ramesh, Magnetoelectric coupling effects in multiferroic complex oxide composite structures, Advanced Materials 22 (2010) 2900–2918. URL: https://onlinelibrary.wiley.com/doi/abs/10.1002/adma.200904326. doi:https://doi.org/10.1002/adma.200904326. arXiv:https://onlinelibrary.wiley.com/doi/pdf/10.1002/adma.200904326.

[13] W. F. Brown, R. M. Hornreich, S. Shtrikman, Upper bound on the magnetoelectric susceptibility, Phys. Rev. 168 (1968) 574–577. URL: https://link.aps.org/doi/10.1103/PhysRev.168.574. doi:10.1103/PhysRev.168.574.

[14] W. Eerenstein, M. Wiora, J. L. Prieto, J. F. Scott, N. D. Mathur, Giant sharp and persistent converse magnetoelectric effects in multiferroic epitaxial heterostructures, Nature Materials 6 (2007) 348–351. URL: https://doi.org/10.1038/nmat1886. doi:10.1038/nmat1886.

[15] S. Priya, R. Islam, S. Dong, D. Viehland, Recent advancements in magnetoelectric particulate and laminate composites, Journal of Electroceramics 19 (2007) 149–166. URL: https://doi.org/10.1007/s10832-007-9042-5. doi:10.1007/s10832-007-9042-5.

[16] J. van Suchtelen, Product properties: a new application of composite materials, Technical Report 27, Phillips Res. Rep, 1972.

[17] R. A. Islam, S. Priya, Effect of piezoelectric grain size on magnetoelectric coefficient of pb(zr0.52ti0.48)o3–ni0.8zn0.2fe2o4 particulate composites, Journal of Materials Science 43 (2008) 3560–3568.

[18] M. Zeng, J. G. Wan, Y. Wang, H. Yu, J.-M. Liu, X. P. Jiang, C. W. Nan, Resonance magnetoelectric effect in bulk composites of lead zirconate titanate and nickel ferrite, Journal of Applied Physics 95 (2004) 8069–8073. URL: https://doi.org/10.1063/1.1739531. doi:10.1063/1.1739531. arXiv:https://doi.org/10.1063/1.1739531.

[19] J. Ryu, S. Priya, A. V. Carazo, K. Uchino, H.-E. Kim, Effect of the magnetostrictive layer on magnetoelectric properties in lead zirconate titanate/terfenol-d laminate composites, Journal of the American Ceramic Society 84 (2001) 2905–2908. URL: https://ceramics.onlinelibrary.wiley.com/doi/abs/10.1111/j.1151-2916.2001.tb01
doi:https://doi.org/10.1111/j.1151-2916.2001.tb01113.x.
arXiv:https://ceramics.onlinelibrary.wiley.com/doi/pdf/10.1111/j.1151-2916.200

[20] M. Li, J. Gao, Y. Wang, D. Gray, J. Li, D. Viehland, Enhancement in magnetic field sensitivity and reduction in equivalent magnetic noise by magnetoelectric laminate stacks, Journal of Applied Physics 111 (2012) 104504. URL: https://doi.org/10.1063/1.4718441. doi:10.1063/1.4718441. arXiv:https://doi.org/10.1063/1.4718441.

[21] C.-W. Nan, Magnetoelectric effect in composites of piezoelectric and piezomagnetic phases, Phys. Rev. B 50 (1994) 6082–6088. URL: https://link.aps.org/doi/10.1103/PhysRevB.50.6082. doi:10.1103/PhysRevB.50.6082.

[22] C. Nan, Y. Lin, J. H. Huang, Magnetoelectricity of multiferroic composites, Ferroelectrics 280 (2002) 153–163. URL: https://www.tandfonline.com/doi/abs/10.1080/713716549.
doi:10.1080/713716549. arXiv:https://www.tandfonline.com/doi/pdf/10.1080/71371654

[23] C.-W. Nan, G. Liu, Y. Lin, H. Chen, Magnetic-field-induced electric polarization in multiferroic nanostructures, Phys. Rev. Lett. 94 (2005) 197203. URL: https://link.aps.org/doi/10.1103/PhysRevLett.94.197203.
doi:10.1103/PhysRevLett.94.197203.

[24] E. Pan, Three-dimensional green's functions in anisotropic magneto-electro-elastic bimaterials, Zeitschrift für angewandte Mathematik und Physik ZAMP 53 (2002) 815–838. URL: https://doi.org/10.1007/s00033-002-8184-1. doi:10.1007/s00033-002-8184-1.

[25] X. Wang, Y.-P. Shen, The general solution of three-dimensional problems in magnetoelectroelastic media, International Journal of Engineering Science 40 (2002) 1069–1080. URL: https://www.sciencedirect.com/science/article/pii/S002072250200006X. doi:https://doi.org/10.1016/S0020-7225(02)00006-X.

[26] G. Harshe, J. Dougherty, R. Newnham, Theoretical modelling of multilayer magnetoelectric composites, Int. J. Appl. Electromagn. Mater. 4 (1993) 145–159.

[27] M. Avellaneda, G. Harshé, Magnetoelectric effect in piezoelectric/magnetostrictive multilayer (2-2) composites, Journal of Intelligent Material Systems and Structures 5 (1994) 501–513. URL: https://doi.org/10.1177/1045389X9400500406. doi:10.1177/1045389X9400500406. arXiv:https://doi.org/10.1177/1045389X9400500406.

[28] G. Wu, T. Nan, R. Zhang, N. Zhang, S. Li, N. X. Sun, Inequivalence of direct and converse magnetoelectric coupling at electromechanical resonance, Applied Physics Letters 103 (2013) 182905. URL: https://doi.org/10.1063/1.4827875. doi:10.1063/1.4827875. arXiv:https://doi.org/10.1063/1.4827875.

[29] T. I. Muchenik, E. J. Barbero, Charge, voltage, and work-conversion formulas for magnetoelectric laminated composites, Smart Materials and Structures 24 (2015) 025039. URL: https://doi.org/10.1088/0964-1726/24/2/025039. doi:10.1088/0964-1726/24/2/025039.

[30] R. Newnham, D. Skinner, L. Cross, Connectivity and piezoelectric-pyroelectric composites, Materials Research Bulletin 13 (1978) 525–536. URL: https://www.sciencedirect.com/science/article/pii/0025540878901617. doi:https://doi.org/10.1016/0025-5408(78)90161-7.

[31] T.-Z. Wang, Y.-H. Zhou, A theoretical study of nonlinear magnetoelectric effect in magnetostrictive–piezoelectric trilayer, Composite Structures 93 (2011) 1485–1492. URL: https://www.sciencedirect.com/science/article/pii/S0263822310004058. doi:https://doi.org/10.1016/j.compstruct.2010.12.003.

[32] L. Lin, Y. Wan, F. Li, An analytical nonlinear model for laminate multiferroic composites reproducing the dc magnetic bias dependent magnetoelectric properties, IEEE Transactions on Ultrasonics, Ferroelectrics, and Frequency Control 59 (2012) 1568–1574. doi:10.1109/TUFFC.2012.2356.

[33] D. Burdin, D. Chashin, N. Ekonomov, L. Fetisov, Y. Fetisov, G. Sreenivasulu, G. Srinivasan, Nonlinear magneto-electric effects in ferromagnetic-piezoelectric composites, Journal of Magnetism and Magnetic Materials 358-359 (2014) 98–104. URL: https://www.sciencedirect.com/science/article/pii/S0304885314000730. doi:https://doi.org/10.1016/j.jmmm.2014.01.062.

[34] Y. Shi, N. Li, Y. Wang, J. Ye, An analytical model for nonlinear magnetoelectric effect in laminated composites, Composite Structures 263 (2021) 113652. URL: https://www.sciencedirect.com/science/article/pii/S0263822321001136. doi:https://doi.org/10.1016/j.compstruct.2021.113652.

[35] M. I. Bichurin, V. M. Petrov, G. Srinivasan, Theory of low-frequency magnetoelectric coupling in magnetostrictive-piezoelectric bilayers, Phys. Rev. B 68 (2003) 054402. URL: https://link.aps.org/doi/10.1103/PhysRevB.68.054402. doi:10.1103/PhysRevB.68.054402.

[36] S. Dong, J.-F. Li, D. Viehland, Longitudinal and transverse magnetoelectric voltage coefficients of magnetostrictive/piezoelectric laminate composite: theory, IEEE Transactions on Ultrasonics, Ferroelectrics, and Frequency Control 50 (2003) 1253–1261. doi:10.1109/TUFFC.2003.1244741.

[37] S. Dong, J. Zhai, Equivalent circuit method for static and dynamic analysis of magnetoelectric laminated composites, Chinese Science Bulletin 53 (2008) 2113–2123. URL:

https://doi.org/10.1007/s11434-008-0304-7. doi:10.1007/s11434-008-0304-7.

[38] Y. Benveniste, Magnetoelectric effect in fibrous composites with piezoelectric and piezomagnetic phases, Phys. Rev. B 51 (1995) 16424–16427. URL: https://link.aps.org/doi/10.1103/PhysRevB.51.16424. doi:10.1103/PhysRevB.51.16424.

[39] J.-Y. Kim, Micromechanical analysis of effective properties of magneto-electro-thermo-elastic multilayer composites, International Journal of Engineering Science 49 (2011) 1001–1018. URL: https://www.sciencedirect.com/science/article/pii/S0020722511001145. doi:https://doi.org/10.1016/j.ijengsci.2011.05.012.

[40] K. Jin, J. Aboudi, Macroscopic behavior prediction of multiferroic composites, International Journal of Engineering Science 94 (2015) 226–241. URL: https://www.sciencedirect.com/science/article/pii/S0020722515000877. doi:https://doi.org/10.1016/j.ijengsci.2015.06.002.

[41] H. Xu, Y. Pei, F. Li, D. Fang, A multi-scale and multi-field coupling nonlinear constitutive theory for the layered magnetoelectric composites, Journal of the Mechanics and Physics of Solids 114 (2018) 143–157. URL: https://www.sciencedirect.com/science/article/pii/S0022509617308049. doi:https://doi.org/10.1016/j.jmps.2018.02.016.

[42] J. Zhang, C. Fang, G. J. Weng, Direct and converse nonlinear magnetoelectric coupling in multiferroic composites with ferromagnetic and ferroelectric phases, Proceedings of the Royal Society A: Mathematical, Physical and Engineering Sciences 475 (2019) 20190002. URL: https://royalsocietypublishing.org/doi/abs/10.1098/rspa.2019.0002. doi:10.1098/rspa.2019.0002. arXiv:https://royalsocietypublishing.org/doi/pdf/10.109

[43] J. Y. Li, M. L. Dunn, Micromechanics of magnetoelectroelastic composite materials: Average fields and effective behavior, Journal of Intelligent Material Systems and Structures 9 (1998) 404–416. URL: https://doi.org/10.1177/1045389X9800900602. doi:10.1177/1045389X9800900602. arXiv:https://doi.org/10.1177/1045389X9800900602.

[44] S. Srinivas, J. Y. Li, The effective magnetoelectric coefficients of polycrystalline multiferroic composites, Acta Materialia 53 (2005) 4135–4142. URL: https://www.sciencedirect.com/science/article/pii/S1359645405002946. doi:https://doi.org/10.1016/j.actamat.2005.05.014.

[45] T. Tang, W. Yu, Variational asymptotic homogenization of heterogeneous electromagnetoelastic materials, International Journal of Engineering Science 46 (2008) 741–757. URL: https://www.sciencedirect.com/science/article/pii/S0020722508000359. doi:https://doi.org/10.1016/j.ijengsci.2008.03.002.

[46] T. Tang, W. Yu, Micromechanical modeling of the multiphysical behavior of smart materials using the variational asymptotic method, Smart Materials and Structures 18 (2009) 125026. URL: https://doi.org/10.1088/0964-1726/18/12/125026. doi:10.1088/0964-1726/18/12/125026.

[47] J. H. Huang, Analytical predictions for the magnetoelectric coupling in piezomagnetic materials reinforced by piezoelectric ellipsoidal inclusions, Phys. Rev. B 58 (1998) 12–15. URL: https://link.aps.org/doi/10.1103/PhysRevB.58.12. doi:10.1103/PhysRevB.58.12.

[48] J. Y. Li, M. L. Dunn, Anisotropic coupled-field inclusion and inhomogeneity problems, Philosophical Magazine A 77 (1998) 1341–1350. URL: https://doi.org/10.1080/01418619808214256. doi:10.1080/01418619808214256. arXiv:https://doi.org/10.1080/01418619808214256.

[49] G. R. Buchanan, Layered versus multiphase magneto-electro-elastic composites, Composites Part B: Engineering 35 (2004) 413–420. URL: https://www.sciencedirect.com/science/article/pii/S1359836804000332. doi:https://doi.org/10.1016/j.compositesb.2003.12.002.

[50] N. Galopin, X. Mininger, F. Bouillault, L. Daniel, Finite element modeling of magnetoelectric sensors, IEEE Transactions on Magnetics 44 (2008) 834–837. doi:10.1109/TMAG.2008.915781.

[51] J. Lee, J. G. Boyd, D. C. Lagoudas, Effective properties of three-phase electro-magneto-elastic composites, International Journal of Engineering Science 43 (2005) 790–825. URL:

https://www.sciencedirect.com/science/article/pii/S0020722505000820. doi:https://doi.org/10.1016/j.ijengsci.2005.01.004.

[52] A. Avakian, R. Gellmann, A. Ricoeur, Nonlinear modeling and finite element simulation of magnetoelectric coupling and residual stress in multiferroic composites, Acta Mechanica 226 (2015) 2789–2806. URL: https://doi.org/10.1007/s00707-015-1336-0. doi:10.1007/s00707-015-1336-0.

[53] J. Zhang, X. Wang, X. Chen, H. Du, G. J. Weng, Finite element analysis of the magnetoelectric effect on hybrid magnetoelectric composites, Composite Structures 296 (2022) 115876. URL: https://www.sciencedirect.com/science/article/pii/S0263822322006432. doi:https://doi.org/10.1016/j.compstruct.2022.115876.

[54] Q. Chen, A. Konrad, A review of finite element open boundary techniques for static and quasi-static electromagnetic field problems, IEEE Transactions on Magnetics 33 (1997) 663–676. doi:10.1109/20.560095.

[55] X. Brunotte, G. Meunier, J. Imhoff, Finite element modeling of unbounded problems using transformations: a rigorous, powerful and easy solution, IEEE Transactions on Magnetics 28 (1992) 1663–1666. doi:10.1109/20.124021.

[56] H. L. Rakotoarison, V. Ardon, O. Chadebec, B. Delinchant, S. Guerin, J.-L. Coulomb, Formal sensitivity computation of magnetic moment method, IEEE Transactions on Magnetics 44 (2008) 1014–1017. doi:10.1109/TMAG.2007.915294.

[57] G. Meunier, J. Coulomb, S. Salon, L. Krahenbul, Hybrid finite element boundary element solutions for three dimensional scalar potential problems, IEEE Transactions on Magnetics 22 (1986) 1040–1042. URL: http://ieeexplore.ieee.org/document/1064625/. doi:10.1109/TMAG.1986.1064625.

[58] T. T. Nguyen, F. Bouillault, L. Daniel, X. Mininger, Finite element modeling of magnetic field sensors based on nonlinear magnetoelectric effect, Journal of Applied Physics 109 (2011) 084904. URL: https://doi.org/10.1063/1.3553855. doi:10.1063/1.3553855. arXiv:https://doi.org/10.1063/1.3553855.

[59] H. Talleb, Z. Ren, Finite element modeling of magnetoelectric laminate composites in considering nonlinear and load effects for energy harvesting, Journal of Alloys and Compounds 615 (2014) 65–74. URL: https://www.sciencedirect.com/science/article/pii/S0925838814014777. doi:https://doi.org/10.1016/j.jallcom.2014.06.121.

[60] Handbook of Giant Magnetostrictive Materials, Elsevier, 2000. URL: https://linkinghub.elsevier.com/retrieve/pii/B9780122386404X50141. doi:10.1016/B978-0-12-238640-4.X5014-1.

[61] IEEE Standard on Magnetostrictive Materials: Piezomagnetic Nomenclature, Technical Report, IEEE, ???? URL: http://ieeexplore.ieee.org/document/19418/. doi:10.1109/IEEESTD.1971.119885.

[62] A. T. Phung, O. Chadebec, P. Labie, Y. Le Floch, G. Meunier, Automatic cuts for magnetic scalar potential formulations, IEEE Transactions on Magnetics 41 (2005) 1668–1671. doi:10.1109/TMAG.2005.846105.

[63] J. Bastos, N. Sadowski, Electromagnetic Modeling by Finite Element Methods, CRC Press, 2003. doi:10.1201/9780203911174.

[64] Y. Saad, Iterative Methods for Sparse Linear Systems, second ed., Society for Industrial and Applied Mathematics, 2003. doi:10.1137/1.9780898718003.

[65] J. Poblet-Puig, A. Rodríguez-Ferran, Modal-based prediction of sound transmission through slits and openings between rooms, Journal of Sound and Vibration 332 (2013) 1265–1287. doi:https://doi.org/10.1016/j.jsv.2012.09.044.

[66] P. Amestoy, I. Duff, J.-Y. L'Excellent, Multifrontal parallel distributed symmetric and unsymmetric solvers, Computer Methods in Applied Mechanics and Engineering 184 (2000) 501–520. URL: https://www.sciencedirect.com/science/article/pii/S004578259900242X. doi:https://doi.org/10.1016/S0045-7825(99)00242-X.

[67] E. Durand, L. de Broglie, Électrostatique et magnétostatique, Masson, 1953.

[68] T. A. Do, H. Talleb, A. Gensbittel, Z. Ren, Homogenization of Magnetoelectric 0–3 Type Composites by 3-D Multiphysics Finite-Element Modeling, IEEE Transactions on Magnetics 55 (2019) 1–4. URL: https://ieeexplore.ieee.org/document/8661774/. doi:10.1109/TMAG.2019.2900149.

[69] V. Loyau, V. Morin, G. Chaplier, M. LoBue, F. Mazaleyrat, Magnetoelectric effect in layered ferrite/PZT composites. Study of the demagnetizing effect on the magnetoelectric behavior, Journal of Applied Physics 117 (2015) 184102. URL: http://aip.scitation.org/doi/10.1063/1.4919722. doi:10.1063/1.4919722.